4-1-2016

Prefrontal White Matter Pathology in Air Pollution Exposed Mexico City Young Urbanites and Their Potential Impact on Neurovascular Unit Dysfunction and the Development of Alzheimer's Disease

Partha S. Mukherjee
Boise State University

Publication Information

Mukherjee, Partha S. (2016). "Prefrontal White Matter Pathology in Air Pollution Exposed Mexico City Young Urbanites and Their Potential Impact on Neurovascular Unit Dysfunction and the Development of Alzheimer's Disease". *Environmental Research, 146*, 404-417. doi: 10.1016/j.envres.2015.12.031

Prefrontal white matter pathology in air pollution exposed Mexico City young urbanites and their potential impact on neurovascular unit dysfunction and the development of Alzheimer's disease.

Lilian Calderón-Garcidueñas[1, 2], Rafael Reynoso-Robles[3], Javier Vargas- Martínez[2], Aline Gómez-Maqueo-Chew [4], Beatriz Pérez-Guillé [3], Partha S. Mukherjee [5], Ricardo Torres-Jardón [6], George Perry [7], Angélica Gónzalez-Maciel [3]

[1] The University of Montana, Missoula, MT 59812, USA

[2] Universidad del Valle de México, Mexico City, 04850, México

[3] Instituto Nacional de Pediatría, Mexico City, 04530 México

[4] Universidad del Valle de México, Hermosillo, Sonora, 83299, México

[5]Mathematics Department, Boise State University, Boise, Idaho, USA

[6] Centro de Ciencias de la Atmósfera, Universidad Nacional Autónoma de México, Mexico City, 04310, México

[7] College of Sciences, University of Texas at San Antonio, San Antonio, TX, USA

Running head: Prefrontal white matter, children, dogs and air pollution

Corresponding author: Lilian Calderón-Garcidueñas MA, MD, PhD, The University of Montana, 287 Skaggs Building, 32 Campus Drive, Missoula, MT, USA 59812 Phone: 406-243-4785 E mail: **lilian.calderon-garciduenas@umontana.edu**

Highlights

- The prefrontal white matter is a target of air pollution
- Tight junctions, key neurovascular unit elements, are abnormal in young urbanites
- Identifying neurovascular dysfunction biomarkers is key for pediatric neuroprotection
- Early characterization of NVU damage may provide a fresh insight into AD pathogenesis

ABSTRACT

Millions of urban children are chronically exposed to high concentrations of air pollutants, i.e., fine particulate matter ($PM_{2.5}$) and ozone, associated with increased risk for Alzheimer's disease. Compared with children living with clear air those in Mexico City (MC) exhibit systemic, brain and intrathecal inflammation, low CSF $A\beta_{42,}$ breakdown of the BBB, attention and short-term memory deficits, prefrontal white matter hyperintensities, damage to epithelial and endothelial barriers, tight junction and neural autoantibodies, and Alzheimer and Parkinson's hallmarks. The prefrontal white matter is a target of air pollution. We examined by light and electron microscopy the prefrontal white matter of MC dogs (n: 15, age 3.17±0.74 years), children and teens (n: 34, age: 12.64±4.2 years) versus controls. Major findings in MC residents included leaking capillaries and small arterioles with extravascular lipids and erythrocytes, lipofuscin in pericytes, smooth muscle and endothelial cells (EC), thickening of cerebrovascular basement membranes with small deposits of amyloid, patchy absence of the perivascular glial sheet, enlarged Virchow-Robin spaces and nanosize particles (20-48 nm) in EC, basement membranes, axons and dendrites. Tight junctions, a key component of the neurovascular unit (NVU) were abnormal in MC versus control dogs (χ^2 <0.0001), and white matter perivascular damage was significantly worse in MC dogs (p= 0.002). The integrity of the NVU, an interactive network of vascular, glial and neuronal cells is compromised in MC young residents. Characterizing the early NVU damage and identifying biomarkers of neurovascular dysfunction may provide a fresh insight into Alzheimer pathogenesis and open opportunities for pediatric neuroprotection.

KEY WORDS: *Air pollution, Alzheimer, BBB, children, dogs, endothelial damage, $PM_{2.5}$,nanosize particles, neurovascular unit, tight junctions.*

Financial support: None

Conflict of Interest: None

1. Introduction

Clinically healthy Mexico City (MC) children with no known risk factors for neurological or cognitive disorders exhibit cognition deficits, brain metabolic, structural and volumetric changes and the neuropathological and cerebrospinal fluid (CSF) laboratory hallmarks of Alzheimer and Parkinson's diseases i.e., tau hyperphosphorylation with pre-tangles, amyloid beta42 (Aβ42) plaques, low CSF Aβ42, and misfolded α-synuclein accumulation (Calderón-Garcidueñas et al., 2008a,2010, 2011a, 2012a, 2013a,2015a).

Brain MRI and MRS studies in MC children and teens versus low air pollution controls show white matter metabolic changes and prefrontal white matter hyperintensities (WMH) (Warlow et al., 2013; Calderón-Garcidueñas et al., 2008b, 2011b, 2012b, 2015a,b), while neuropathology findings reveal cortical disruption of the blood-brain barrier (BBB), endothelial activation, oxidative stress, high concentration of metals associated with combustion, inflammatory cell trafficking along with up-regulated gene network clusters including IL1, NFκB, TNF, IFN, and TLRs (Calderón-Garcidueñas et al., 2003, 2008a,2009a, 2010, 2011a,2013a,b). Animal facility healthy MC young dogs also exhibit WMH by MRI, neuroinflammation, DNA oxidative damage, BBB breakdown, and accumulation of combustion-related metals (Calderón-Garcidueñas et al., 2002, 2003,2008b, 2009a). The prefrontal cortex is a target of air pollution and its damage likely a major contributor to cognitive deficits in Mexico City young residents. Prior research has shown all epithelial and endothelial barriers are compromised in MC children

and dogs and the production of high concentrations of endothelin- 1 and autoantibodies against tight junction and neural proteins could be playing a role in the diffuse microvascular changes observed in young urbanites (Calderón-Garcidueñas et al., 2001, 2007, 2008c, 2009b, 2015d). In a recent study of 139 clinically healthy MC and control children age 11.91 ± 4.2 y, serum antibodies against occludin/zonulin 1 and actin IgG, along with myelin oligodendrocyte glycoprotein, myelin basic protein, S-100, and cerebellar IgG were significantly higher in MC children (Calderón-Garcidueñas et al., 2015d). Zonula occludens (ZO) proteins are at the core of the protein networks which are anchored to the TJ-plaque dynamic structures and given that neuroinflammation is associated with BBB dysfunction and loss of tight junctions (Bauer et al., 2014; Elahy et al., 2015;Haseloff et al., 2015), we fully expected brain structural and metabolic changes in MC children.

Extensive data in the literature support human and animal breakdown of the nasal/olfactory, BBB and alveolar-capillary barriers and the expression of detrimental genes associated to urban air pollution (Harkema et al.,2006; Ljubimova et al., 2013; Van Miert et al., 2005; Kaplan et al., 2010; Kish et al., 2013; Carson et al., 2013; Bergin and Witzmann, 2013; Garwood et al., 2014). The work by Kamat, Winkler, Hawkes, Cabezas, Garwood et al., (2014) is of particular interest to us given that their research support damage to brain endothelial cells occurs early in relation to Alzheimer's neuropathology and BBB disruption leads to neuronal damage, reactive gliosis, oxidative stress, neuroinflammation and early neurovascular dysfunction.

Of great concern in polluted environments with high concentrations of ultrafine particulate matter (UFPM, nanosize particles < 100 nm) is that after passage through biological barriers, UFPM end up in contact with the vascular endothelium and can induce damage (Wang et al.,

2009; Gehr et al., 2011; Sharma et al., 2013; Ucciferri et al., 2014; Karmakar et al., 2014; Meng et al., 2015). The presence of high affinity autoantibodies against barrier forming proteins in urban children are critical to our understanding of air pollutant mechanistic damage pathways. There is robust evidence nanosize particles can increase endothelial paracellular permeability *in vitro* and induce endothelial TJ opening (Sharma et al., 2013; Yu et al., 2013; Ucciferri et al., 2014; Karmakar et al., 2014; Li et al., 2015).

The developing brain relies heavily on the delivery of oxygen and nutrients from the blood stream to meet metabolic demands of neural cells and blood supply, thus neural activity and vascular dynamics are tightly coupled (Lecrux and Hamel, 2011; Lacoste and Gu, 2015).The neurovascular unit (NVU) is the anatomical substrate of neurovascular interactions and a complex interaction between endothelial cells, pericytes, astrocytes, microglia and neurons is responsible for optimal delivery of oxygen and nutrients to the brain (Simard et al., 2003; Zlokovic, 2008; Lo and Rosenberg, 2009; Lacoste and Gu, 2015).A key function of this system is to keep a tightly control environment aimed to preserve the brain from toxins, pathogens and harmful chemicals. Neurovascular dysfunction has a relevant focus in Alzheimer's disease (AD) research, particularly regarding BBB integrity, cerebral blood flow (CBF) and glucose transport into the brain (Iadecola, 2004; Keaney and Campbell, 2015; Sweeney et al., 2015). White matter abnormalities are common in dementia and the pathology is the result of a combination of structural alterations of the cerebral vasculature, i.e., arteriolosclerosis, cerebrovascular basement membrane pathology, and amyloid angiopathy, and nonstructural vascular abnormalities (vascular contractility or permeability) and/or neurovascular instability (Love and Miners 2015).

Very little is known regarding the ultrastructural features of tight junctions (TJs), cerebrovascular basement membranes (Morris et al., 2014), capillaries, arterioles and axons in the prefrontal white matter of young healthy dogs and children with a lifetime exposure to urban air pollution. Our working hypothesis states that healthy, young dogs will have prefrontal vascular and white matter pathology and children living in the same area will share light and electron microscopic (EM) findings with those of dogs' raised in an animal facility in Mexico City.

We have one aim for this study: To document by 1 μm toluidine blue thick sections and EM the integrity of the prefrontal white matter in healthy young dogs resident in MC (n: 9) and in a cohort of MC children and teens (n: 26) autopsy prefrontal samples versus clean air controls (6 dogs and 8 children). Stored brain samples from seemingly healthy children dying suddenly in accidental deaths not involving the cranial cavity and undergoing forensic autopsies were the source of the frontal samples.

Our results identify abnormalities at the endothelial junctional complexes, microbleeds, perivascular lipid accumulation, abnormal cerebrovascular basement membranes, and the presence of ultrafine particles in mitochondria, basement membranes, axons and dendrites. Our study suggests that the integrity of the NVU in the prefrontal white matter is compromised in highly exposed young urbanites and short and long-term brain health consequences are expected.

2. PROCEDURE

2.1. Study Cities and Air Quality

Children's cohorts were selected from the Mexico City Metropolitan Area (MCMA)

and control locations consisting of small cities in Mexico (Zacatlán and Huachinango, Puebla; Zitácuaro, Michoacán; Puerto Escondido, Oaxaca). The control cities have <75,000 inhabitants and because of their small size their levels for the main criteria air pollutants (ozone, particulate matter, sulfur dioxide, nitrogen oxides and carbon monoxide) are lower than the current US EPA standards (Alonso et al., 2007; Semarnat, 2012).

Mexico City Metropolitan Area is an example of extreme urban growth and accompanying environmental pollution (Bravo-Alvarez and Torres-Jardón, 2002; Molina et al., 2010; Retama et al., 2015). The metropolitan area of over 2,000 km^2 lies in an elevated basin 2,200 m above sea level surrounded on three sides by mountain ridges. MCMA's nearly 24 million inhabitants, over 50,000 industries, and 5.5 million vehicles consume more than 50 million liters of petroleum fuels per day, producing an estimated annual emission of 2.3 million tons of particulate and gaseous air pollutants. MCMA motor vehicles produce abundant amounts of primary fine particulate matter ($PM_{2.5}$). The high altitude and tropical climate where the MCMA is settled facilitate ozone production all year and contribute to the formation of $PM_{2.5}$. Children from MCMA were residents in the northern-industrialized and southern-residential zones. Northern children have been exposed to higher concentrations of volatile and toxic organic compounds, PM_{10}, and $PM_{2.5}$ including high levels of its constituents: organic and elemental carbon, nitro- and polycyclic aromatic hydrocarbons and metals (Zn, Cu, Pb, Ti, Mn, Sn, V, Ba), while southern children have been exposed continuously to significant and prolonged concentrations of ozone, secondary aerosols (NO_3^-) and particulate matter associated with lipopolysaccharide PM-LPS.

2.2 Subjects

The work described in this research was conducted in accordance with the Code of Ethics involving animal research and the Institutional Animal Care and Use Committees. The frontal dog samples used in this work were obtained previously from two independent studies involving the use of Nimesulide® in mixed beagle dogs and a metal study (Calderón-Garcidueñas et al., 2002, 2003, 2008b, 2009a). Procedures used were in accordance with the guidelines of the Use and Care of Laboratory Animals (NIH Pub No.86-23). The autopsy frontal samples were obtained from forensic cases with no identifiable personal data, not meeting the regulatory definition of human subject research. Autopsies were performed

2.2.1 Animal facility young dogs

Previously harvested dog frontal tissues for EM were used for this study. Two cohorts, one from MC and a control cohort of mixed beagles were whelped and housed in an outdoor-indoor kennel; husbandry was in compliance with the American Association of Laboratory Animal Certification Standards. Dogs were under daily veterinarian observation during their entire life, and at no time there was any evidence of respiratory, cardiovascular, gastrointestinal or neurological diseases. Dogs had all applicable vaccines and were treated with anti-helmintics regularly. Dogs from both cohorts had the same diets. Dogs were sacrificed with an overdose of sodium pentobarbital. Tissue blocks were archived in phosphate-buffered saline 0.1M pH 7.5 with sodium azide at 4°C prior to processing for EM. We selected to use frontal white matter tissue optimally fixed for electron microscopy from 15 dogs (3.17±0.74 years). The 9 Mexico City selected dogs age 3.11±0.67 years were in the non-treated Mexico City group exposed 24/7 to the Southwest MC atmosphere from birth. Six control dogs average age 3.23±0.81 years were also studied (Table 1).

2.2.2 Light microscopy in dog samples

Frontal samples were post-fixed in 1% osmium tetraoxide and embedded in Epon. Semi-thin sections (0.5 to 1μm) were cut and stained with toluidine blue for light microscopic

examination. Thirty blocks from the right (n: 15) and left (n: 15) prefrontal white matter were cut and examined in each dog. Each toluidine blue 1μm section (30 slides in each dog) was examined under a microscope Carl Zeiss Axioskop 2 Plus equipped with a AxioVision REL 4.8 imaging system. For the measurement of abnormal neuropil areas we selected a square of 60 μm^2 and 16 areas of neuropil were reviewed and measured in 4 randomly selected toluidine blue 1μm section slides (2R/2L) in each dog. One EM researcher was in charge of the measurement of the abnormal neuropil areas and the percentage of white matter damage was recorded in each dog, within each cohort, MC versus controls. This researcher in charge of the measurement of all slides was blind to the identification of the dog. A board-certified pathologist (LCG) without access to the identification codes reviewed the sections and the representative pictures.

2.2.3 Examination of dogs' frontal white matter samples by Transmission Electron Microscopy (TEM)

We selected the EM areas from the semi-thin sections stained with toluidine blue. Ultra-thin sections (60-90 nm) were cut and collected on slot grids previously covered with Formvar membrane. Sections were stained with uranyl acetate and lead citrate, and examined with a JEM-1011 (Japan) microscope. Each electron micrograph was evaluated separately, then compared by group. We captured ultrastructural blood vessel images including sites of TJ's complexes, cerebrovascular basement membranes and the neuropil components. An average of 30 consecutive blood vessels and adjacent neuropil from each animal were documented. One EM researcher examined the TJs structures at magnifications between 12,000x to 100,000x, took representative pictures and recorded normal and abnormal endothelial TJ structures from capillaries based on the following characteristics: observation of the endothelial junction

undulated trajectory in a plane parallel to the basement membrane and exhibiting structurally closed and intact TJs as elegantly described by Muir and Peter (1964) and Castejón (2012,2014), open inter-endothelial junctions, and loss of integrity and disruption of TJs.

We also noted astrocyte end feet detachment from the basement membranes, caveolar EC activity, the characteristics of the basement membranes, and microvascular endothelial cell damage including irregularity of the endothelial cell luminal surface, micro-villi like protusions, and bleb-like structures. The comparison between the results of the evaluation of 40 endothelial cell to endothelial cell TJs in each of the 15 animals, including 6 controls was assessed for significance with a chi square test.

2.2.4 Examination of children and teens prefrontal white matter samples by Light and Transmission Electron Microscopy (TEM)

In the process of selecting the frontal samples we examined the entire autopsy in each subject and ruled out the presence of pathological processes other than the lesions associated to the sudden accidental death. The striking difference between dog and human frontal EM samples was the optimal preservation of tissues in dogs v humans given the time between death and autopsy. Given that the neuropil was not optimally preserved for EM in humans, the quantification of abnormal neuropil areas was not done. Frontal samples were post-fixed in 1% osmium tetraoxide and embedded in Epon. Semi-thin sections (0.5 to 1μm) were cut and stained with toluidine blue for light microscopic examination. Thirty blocks from the right (n: 15) and left (n: 15) prefrontal white matter were cut and examined in each child.

2.2.5 Statistical analysis

Statistical analyses were carried out using Excel and R **(**https://www.r-project.org/**).** All data are expressed as mean ±SD. We carried out statistical tests for intergroup differences after adjusting age. We used linear regression technique to accomplish this. We found that the p-values are <0.008 in all 15 white matter areas showing evidence of significant intergroup differences. Next, we tested for the significance of differences between the measurements of tight junction abnormalities in the control and Mexico City group by using the Chi-square test.

3. RESULTS

3.1 Air Quality Data

Mexico City residents are exposed year-round to particulate matter (PM) concentrations above United States National Air Ambient Quality Standards (NAAQS). For this work we focused on inhalable PM, broadly defined by the diameter of the aerodynamic particles, and classified into coarse particles (<10 to >2.5μm; PM_{10}), fine particles (<2.5μm, $PM_{2.5}$) and ultrafine PM (UFPM<100nm). In spite of the efforts by the authorities to control PM air pollution, fine particles are still a health problem in MC because their levels have not shown a reduction trend in the last 10 years. Both, the $PM_{2.5}$ annual air quality standard of 12 μg/m^3 and the 24-hr standard of 35 μg/m^3 have been historically exceeded across the metropolitan area (Figure 1). The highest concentrations occur in the NE sector (Xalostoc) where industrial and traffic activities are prevalent, and decrease towards the SW residential area (Pedregal).

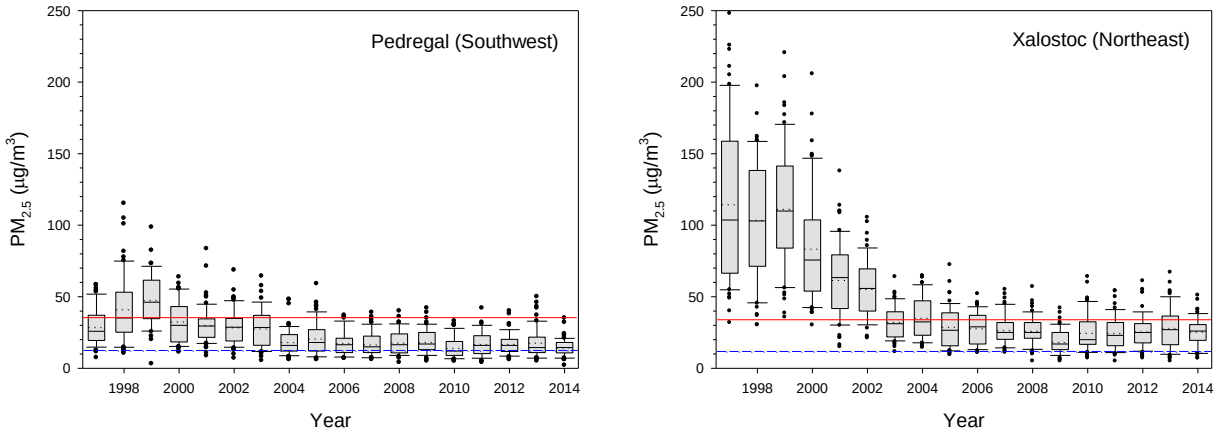

Figures 1 and 2. Box plots for 24-hour $PM_{2.5}$ concentrations at two representative sites of Mexico City Metropolitan Area: Pedregal (residential SW area) and Xalostoc industrial and high traffic (NE area) from 1997 to 2014. The dashed lines inside the boxes are the annual average and the continuous lines the 24-hr median. The $PM_{2.5}$ annual mean NAAQS concentration value is represented by the dashed blue line and the $PM_{2.5}$ 24-hr average NAAQS level is shown with the red continuous line. $PM_{2.5}$ data were not available in MCMA until 2004, thus the $PM_{2.5}$ trends were approximated using a correlation equation of the $PM_{2.5}/PM_{10}$ ratio for the period 2004-2011 and PM_{10} data measured at each site of the period 1997-2003. PM_{10} and $PM_{2.5}$ data were obtained from the Secretaria del Medio Ambiente del Distrito Federal (**http://www.aire.df.gob.mx**).

As Figure 2 shows, North-East MC teenagers older than 15 years old were conceived and born when $PM_{2.5}$ average 24-hr levels were 2 to 3 times the current NAAQS. It should be noticed, every resident in MC has been exposed to $PM_{2.5}$ concentrations above the respective NAAQS regardless of their place of residency within the city. Chemical PM composition studies in Mexico City have shown that the proportion of the different component PM species has not change significantly along the years (Bravo-Alvarez and Torres-Jardón, 2002; Vega et al., 2010; Molina et al., 2010; Retama et al., 2015). Figure 3 shows the chemical composition of coarse (PM_{10}-$PM_{2.5}$) and fine ($PM_{2.5}$ and PM_1) particles in a representative site of MC.

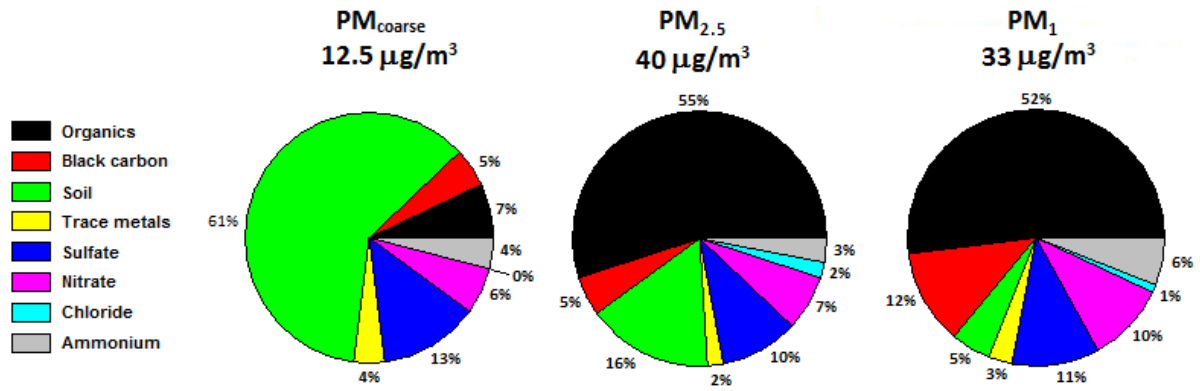

Figure 3. Average mass and composition of PM coarse (PM10–PM2.5), PM2.5 and PM1 at the Instituto Mexicano del Petróleo site (northern Mexico City) during March 2006 (based upon a compilation of Molina et al., 2010, Querol et al., 2008 and Aiken et al., 2009).

In general, PM_{10} in MCMA is dominated by the fine fraction. The $PM_{2.5}/PM_{10}$ ratio variations and the PM chemical composition are dependent on the site location and on the season. The $PM_{2.5}/PM_{10}$ ratio shows relatively lower values at the E and NE sectors relative to the SW sites. Typically, the coarse PM is strongly dominated by geological material (SiO_2+CO_2^{-3} +Al_2O_3+Ca+Fe+Mg+K) from dust resuspension and its proportion diminishes as the particle decreases in size. In contrast, and of key importance for the brain effects, organic and carbonaceous aerosols are the dominant species in the PM fine fraction. Particle emissions from gasoline and Liquefied Petroleum Gas Combustion (LPG) are dominated by organic carbonaceous aerosols (OC), while in diesel particles black carbon (BC) is the key component. OC species include large alkanes, alkanoic acids, benzoic acids, benzaldehydes, phenols, alkanals, etc. (Seinfeld and Pandis, 1998). Contrary to expected, BC concentrations in $PM_{2.5}$ have not shown a decrease through the years (Retama et al., 2015). BC is associated with

polycyclic aromatic compounds (PAHs). PAHs are semivolatile species formed through the fusion of two or more benzene rings by a pyrolitic process during the incomplete combustion of carbonaceous fuels such as gasoline and diesel vehicle exhaust gases. Most of PAHs in MCMA are present in the fine fraction ($PM_{2.5}$) contributing with 75 to 85% of the total mass. In general, low molecular PAHs have a higher ratio than high molecular PAHs in $PM_{2.5}$ (Mújica et al., 2010). On the other hand, secondary inorganic aerosols typically comprise around 20% in all PM_{10} fractions. They are dominated by ammonium sulphate showing the highest levels at the Pedregal southwest area.

Trace metals in fine particles comprises around the 50% of the PM_{10}. The most abundant metals in $PM_{2.5}$ are Zn, Cu, Pb, Ti, Sn, Ba, Mn, Sb, V, Se, As, Ni, Cd, Cr in that order (Querol et al., 2008). Zn, Cu, Ba, Pb, Pb and Cd are tracers of road traffic, while V and Ni are tracers of industrial emissions. MC children in this study have been exposed to significant concentrations of $PM_{2.5}$ during their entire life, including the prenatal period. The high concentrations of $PM_{2.5}$ coincide with the time children play outdoors and/or stay in schools with broken windows and doors and are in close proximity to high traffic and fixed sources of pollution (Villarreal-Calderón et al., 2002). Children are also exposed to ozone concentrations above the USA standards (Calderón-Garcidueñas et al., 2015d). All other criteria pollutants for MCMA, including nitrogen dioxide, sulfur dioxide and lead have been at or below the current EPA standards (Secretaría del Medio Ambiente del Distrito Federal: http://www.aire.df.gob.mx). Control children have been lifelong residents in low pollution cities with all criteria air pollutants below the US EPA NAAQS standards (Calderón-Garcidueñas et al., 2012a).

3.2 Quantification of the abnormal neuropil prefrontal areas in dogs' samples.

Measurement of abnormal neuropil areas showed a significant difference between control and Mexico City dogs matched by age, p= 0.002 (Table 1).

3.3 Light Microscopy and Electron Microscopic dogs' and children results

There was no statistical difference in the selected control versus MC dogs' ages (p= 0.95) Table 1 and control versus MC children (p= 0.93) (Table 2). Children carrying an APOE 4 allele were representative of the population at large (17.6%).The white matter pathology results in Mexico City dogs, children and teens versus controls were divided in 4 sections: 1. One micron toluidine blue light microscopy of blood vessels including capillary, postcapillary venules and arterioles 2. Endothelial ultrastructural pathology, including tight junctions (TJs), pericyte and smooth muscle cell morphology and cerebrovascular basement membranes, 3.Oligodendroglia, axonal, and dendritic electron microscopy and 4. Localization of nanosize particles.

3.3.1 Light microscopy morphological assessment using toluidine blue staining in dog's frontal white matter

Control samples of frontal white matter exhibited normal blood vessels ranging from arterioles, capillaries and venules. Virchow-Robin (VR) spaces were unremarkable and free of mononuclear cells, red blood cells (RBC) or lipid droplets. The neuropil was unremarkable and in particular the myelinated axons varied in size, they were uniformly distributed and intact (Figure 4A). In contrast, Mexico City dogs exhibit expanded VR spaces with mononuclear cells characterized by large nuclei with increased chromatin condensation (Figure 4B). We observed patchy pallor of the neuropil with zones where the myelinated axons were scanty and alternated with clusters of small myelinated fibers (Figure 4C), along extensive areas of rarefaction of the

neuropil around blood vessels (Figure 4D*). Large perivascular cells with the morphology of macrophages and clusters of lipid droplets were prominent around blood vessels (Figure 4E, 4F). Distributed throughout the frontal white matter, small blood vessels exhibit hyperplastic endothelial cells reducing their lumen (Figure 4G). In the transition between the subcortical white and the gray matter, abnormal small vessels were also present with RBC occupying the perivascular space (Figure 4H). Remarkably, neuronal bodies in the transition area exhibited vacuolated cytoplasm.

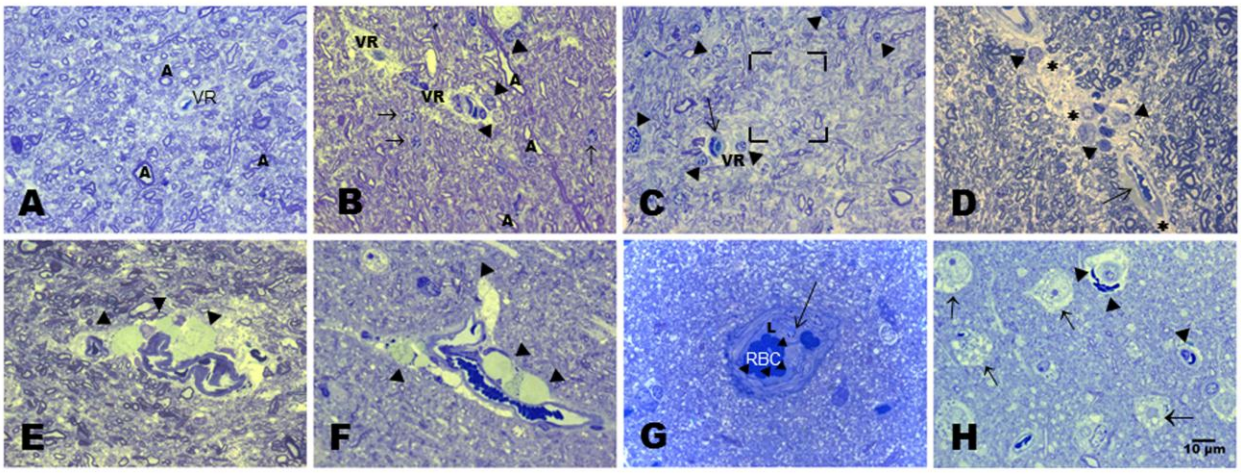

Figure 4. Light microscopy assessment using toluidine blue staining in dog's frontal white matter. Unremarkable white matter is characteristic of control dogs (Figure 4A). Virchow-Robin (VR) spaces are free of mononuclear cells, red blood cells or lipid droplets. The neuropil is unremarkable and the myelinated axons (A) vary in size, they are uniformly distributed and they are

intact. In contrast, Mexico City dogs exhibit expanded VR spaces with mononuclear cells characterized by large nuclei with increased chromatin condensation (Figure 4B, arrowheads). Scattered through the neuropil, cells with large nuclei and increased chromatin condensation are present (Figure 4B short arrows). Patchy pallor of the neuropil with zones where the myelinated axons are scanty and alternate with clusters of small myelinated fibers (Figure 4C square) and cells showing prominent chromatin condensation (Figure 4C arrowheads) are common in MC dogs. Small arterioles show thick walls and expanded VR spaces (long arrows). In Figure 4D we observed extensive areas of rarefaction of the neuropil around blood vessels (*). Large perivascular cells have the morphology of macrophages (arrowheads), while clusters of lipid droplets are prominent around blood vessels (long arrows). In Figure 4E, a close up of a typical blood vessel in a young dog showing large accumulation of lipids (arrowheads). Figure 4F shows a postcapillary venule with perivascular lipid accumulation (arrowheads). Distributed throughout the frontal white matter, small blood vessels (Figure 4G) exhibit hyperplastic endothelial cells (arrowheads) reducing their lumen (L). Mononuclear cells are seen attached to the hyperplastic endothelium (long arrow). In the transition between the subcortical white and gray matter (Figure 4H), abnormal small vessels are also present with RBC occupying the perivascular space (arrowheads). Remarkably, neuronal bodies in the transition area have vacuolated cytoplasm (short arrows).

3.3.2 Light microscopy morphological assessment using toluidine blue staining in children's frontal white matter

Control children exhibited unremarkable blood vessels, Virchow-Robin (VR) spaces and neuropil (Figure 5A). MC children showed significant expansion of the VR spaces and clusters of perivascular lipids (Figures 5B, 5C). Scattered small tortuous blood vessels showed mononuclear cells in the expanded perivascular spaces and leaking of lipid material affected small capillaries (Figure 5D, 5E). A few of the blood vessels architecture was completely lost (Figure 5F). Axonal abnormalities were present and a few large axons show intraaxonal vacuolation and curled membrane fragments. Hyperplastic endothelial cells were common (Figure 5G). In the transition between the subcortical white and the gray matter, abnormal small vessels were present with amorphous material occupying the intra and perivascular spaces (Figure 5H).

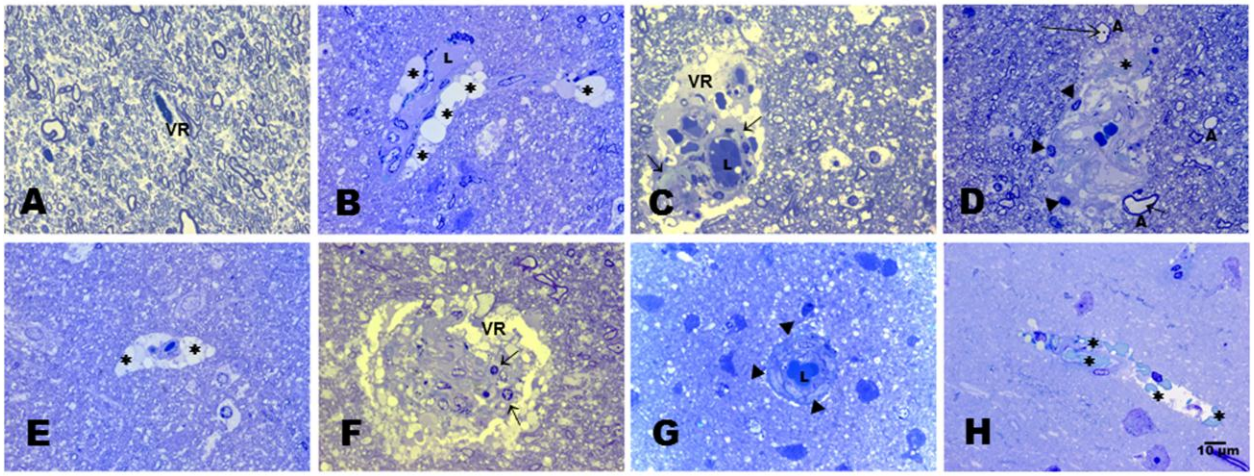

Figure 5. Light microscopy assessment using toluidine blue staining in children's frontal white matter. Control children (Figure 5A) exhibit unremarkable blood vessels, Virchow-Robin (VR) spaces and neuropil. MC children show lipid material accumulation around blood vessels (Figure 5B *) and a significant expansion of the VR space and clusters of perivascular lipids (Figure 5C, short arrows). Scattered small tortuous blood vessels show mononuclear cells (Figure 5D, arrowheads) in the expanded perivascular spaces (*). A few large axons (A) show intraaxonal vacuolation (short arrows) and curled membrane fragments (long arrows). Leaking of lipid material also affects small capillaries (Figure 5E*). A few of the blood vessels architecture is completely lost (Figure 5F). Scattered unidentified cells show clumping of the chromatin (short arrows).Hyperplastic endothelial cells are also seen (Figure 5G, arrowheads). In the transition between the subcortical white and gray matter, abnormal small vessels are present with amorphous material occupying the intra and perivascular spaces (Figure 5H*).

3.3.3. Electron microscopy of dogs' blood vessels and neuropil

Mexico City dogs exhibited abnormal small blood vessels with irregular endothelial basement membranes, RBC in the widened perivascular spaces along with clusters of lipid material and cell fragments (Figures 6A, 6B). Early formation of lipofuscin was a common finding in pericytes of <2y old dogs, while capillaries showed irregular luminal endothelial cell surfaces with microvilli-like protrusions (Figures 6C,6D). Thick and irregular basement membranes were a common finding (Figure 6E). Scattered capillaries showed cells in the position of pericytes and smooth muscle cells with semicircular or circular thickening of vascular walls containing large amounts of amorphous material and smaller areas with amyloid-like fibrils (Figures 6F, 6G). Endothelial cells showed microvilli-like protrusions, prominent endothelial cell nuclei protruding in the lumen and attached white blood cells (WBC) occupying the lumen of the vessels (Figures 6H, 6I).

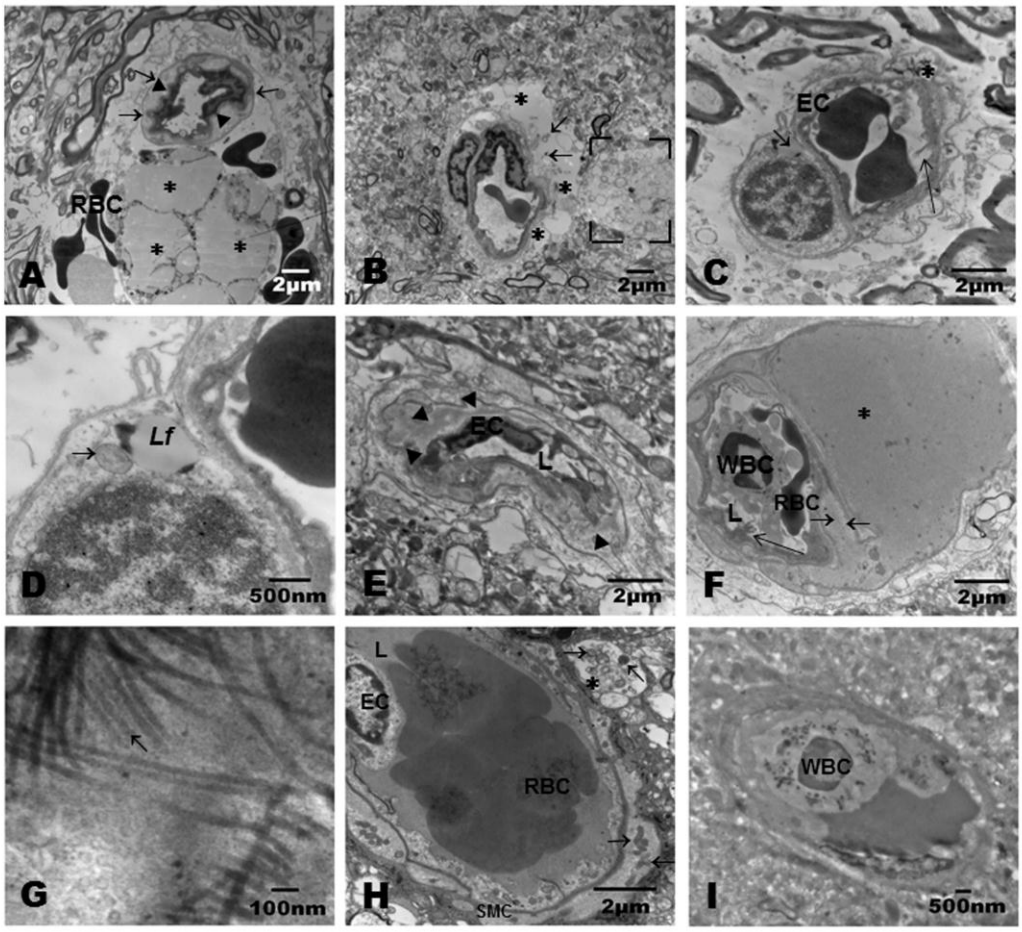

Figure 6. Electron microscopy of dogs' blood vessels. An abnormal small blood vessel (Figure 6A) with irregular endothelial basement membranes (arrowheads) and an apparently intact perivascular glial sheath (short arrows) shows clusters of lipid material (*). RBC are seen in the perivascular space. Figure 6B shows a capillary vessel with a wide perivascular space (*) occupied by cell fragments (short arrows). Note the significant rarefaction of the neuropil on the right side of the picture (square). Early formation of lipofuscin is seen in pericytes of <3y old dogs (Figure 6C short arrow).Capillaries show irregular luminal endothelial cell (EC) surface with microvilli-like protrusions (long arrow) and a large perivascular space with abundant cellular debri (*). A close up of the lipofuscin formation can be seen in Figure 6D. A lipofuscin granule (*Lf*) with dense osmiophilic content, and one mitochondria with abnormal cristae *(*Figure 6D, short arrow*)* lie in the adjacent cytoplasm. In Figure 6E, a small vessel shows a thick and irregular basement membrane (arrowheads). Scattered capillaries show cells in the position of pericytes and smooth muscle cells with semicircular or circular thickening of vascular walls containing large amounts of amorphous material (Figure 6F *) and smaller areas with amyloid-like fibrils (short arrows). The endothelial cell shows microvilli-like

protrusions (long arrow) and there is a white blood cell (WBC) and one RBC occupying the vessel lumen (L). Figure 6G shows helical twist amyloid fibers with a 35-50A repeat(short arrow).A blood vessel with a prominent endothelial cell nucleus (EC) protruding in the lumen is seen in Figure 6H along with RBC.A smooth muscle cell (SMC) cytoplasm display multiple mitochondria (short arrows). An unidentified perivascular structure shows a vacuolated background (*) with cellular fragments (short arrows). A capillary with an attached white blood cell (WBC) occupies the lumen of the vessel (Figure 6I).

White matter arterioles displayed layers of smooth muscle cells (Figures 7A, 7B). Tight junctions between endothelial cells were mostly unremarkable in Mexico City dogs (Figure 7C). A significant number of prefrontal white matter capillaries in highly exposed dogs were characterized by wide VR spaces and the patchy absence of astrocytic perivascular endfeet (Figure 7D). Mononuclear cells commonly occupied the VR space and projected cytoplasmic processes towards the capillary wall while patchy areas of neuropil were characterized by the absence of axons and cellular profiles. Unremarkable tight junctions alternated with the presence of osmiophilic granular material obliterating the cleft of the TJs and focal lack of integrity of the TJs (Figures 7F, 7G). In contrast, control animals displayed unremarkable TJs (Figure 7H). Quantification of the abnormal tight junction in prefrontal endothelial cells yielded a significant difference between control and Mexico City dogs, χ^2 statistic=21.96, degrees of freedom=1, χ^2 <0.0001.

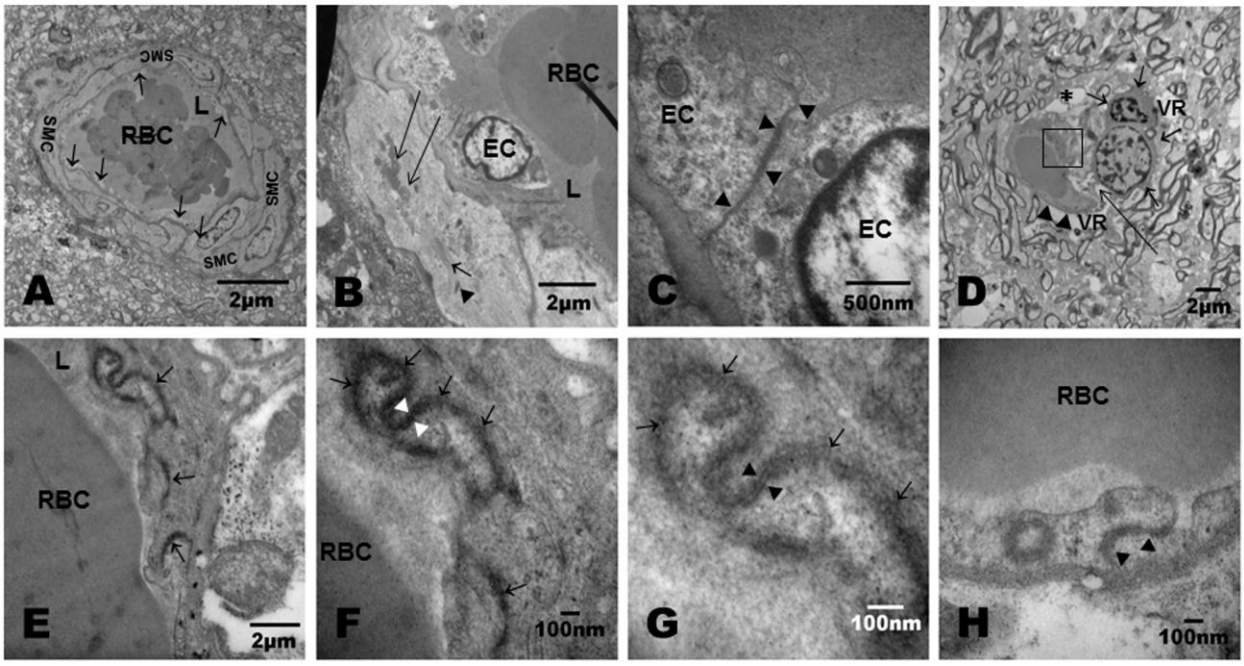

Figure 7. Electron microscopy of dogs' blood vessels. White matter arterioles display layers of smooth muscle cells (SMC)(Figure 7A). Endothelial cells (short arrows) and RBC are seen. In a close-up (Figure 7B), the typical components of a smooth cell cytoplasm are present, bundles of microfilaments (short arrows), elastic microfibrils (arrowheads), dense bodies and mitochondria (long arrows). A close-up of a tight junction between two endothelial cells (EC) is seen in Figure 7C (arrowheads). A significant number of prefrontal white matter capillaries (Figure 7D) in MC dogs are characterized by wide VR spaces and the patchy absence of astrocytic perivascular endfeet (arrowheads). Mononuclear cells (short arrows) occupy the VR space and project cytoplasmic processes towards the capillary wall (long arrows). Patchy areas of neuropil (*) are characterized by the absence of axons and cellular profiles. Figure 7E is a higher power of the square in Fig 7D to focus on tight junctions in endothelial cells. A series of tight junctions (short arrows) between endothelial cells define the limits between cells. A RBC is seen in the lumen of the capillary. A higher power of the TJ's (Figure 7F) illustrates the clear lining of the cleft (white arrowheads) alternating with the presence of osmiophilic granular material obliterating the cleft of the TJs (short arrows). A portion of the RBC is seen in the lumen of the capillary. Higher magnification (150,000 x) shows a TJs intact segment (Figure 7G

arrowhead) and the lack of integrity of the TJ's (short arrows). In Figure 7H a TJs (arrowheads) is intact in a control animal (RBC in lumen).

3.3.4 Electron microscopy of children' blood vessels and neuropil

The typical prefrontal findings in Mexico City children included: small blood vessels with accumulation of lipofuscin in pericytes and undulating irregularly thickened EC basement membranes (Figures 8A, 8B, 8C). Striking isolated arteriolar white matter changes were observed in Mexico City children (Figure 8D). Changes included irregular and thick basement membranes and endothelial cells with large lysosomal bodies (Figure 8E). Interspersed scant pyknotic nuclei were identified in relation with smooth muscle cells. Hyperplastic endothelium associated with a reduction of the lumen, marked thickening of the endothelial basement membranes and extensive perivascular areas of cell debri, vacuolization of the neuropil and abnormal large axons were common findings in MC samples, but not in controls (Figure 8F). Irregular basement membrane varied in thickness between 0.8 to 2 μm (Figures 8G, 8H). Occasionally, we observed the apparent penetration of a mononuclear luminal cell through the endothelium (Figures 8I, 8J) and a poor focal definition of the BM endothelial cell (Figure 8K).

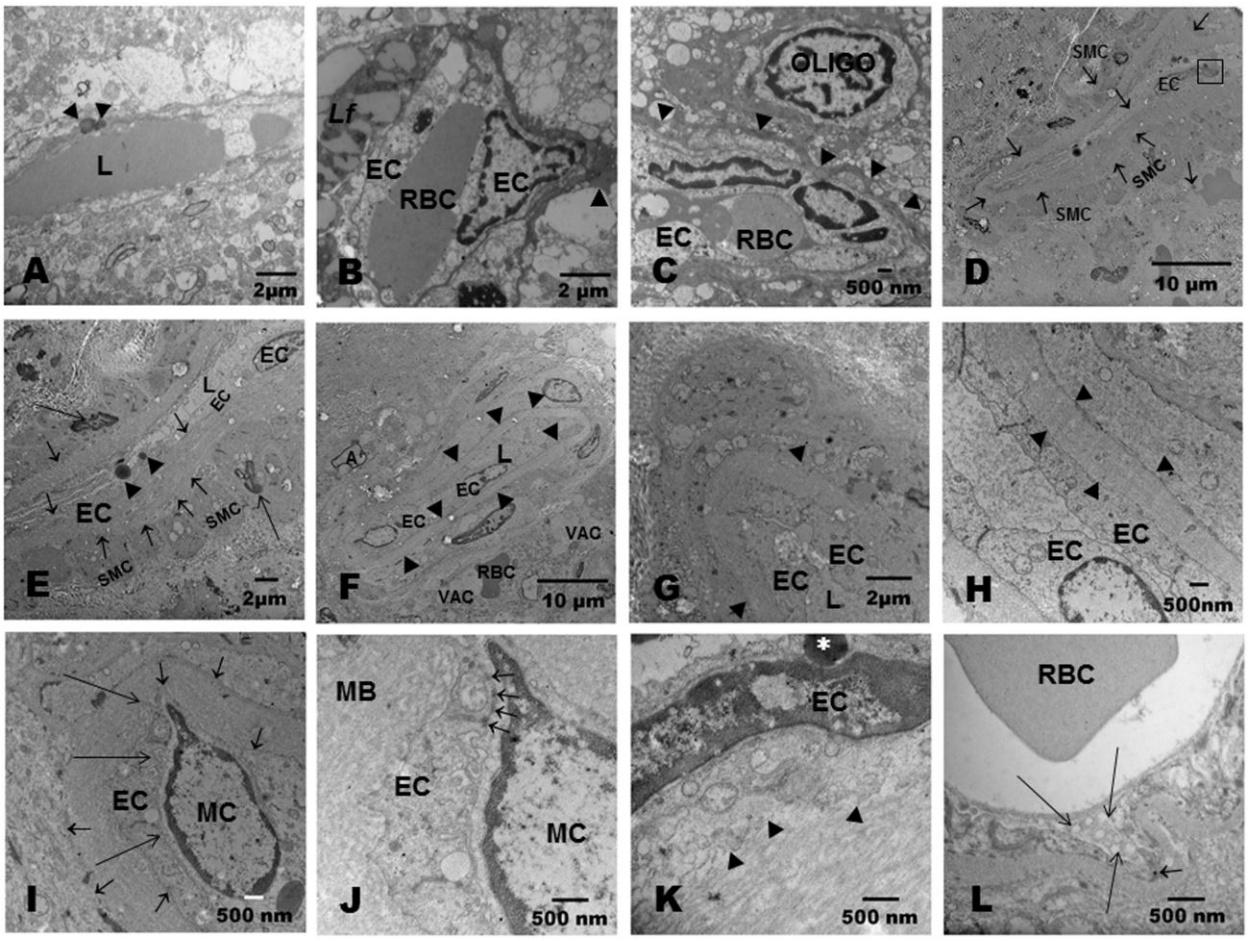

Figure 8. Electron microscopy of children' prefrontal white matter. A prefrontal white matter small blood vessel (Figure 8A) exhibits a typical finding in MC children: accumulation of lipofuscin (arrowheads) in pericytes. Extensive accumulation of lipofuscin (*Lf*) is a major finding in perivascular cells (Figure 8B). A pericyte is present (arrowheads), along with a RBC occupying the entire vessel lumen. In Figure 8C, an olidendroglial cell (OLIGO) is seen adjacent to a small blood vessel with an undulating basement membrane (arrowheads). Striking arteriolar white matter changes are observed in MC teens (Figure 8D). An arteriole exhibits an irregular and thick basement membrane (short arrows) between the endothelial cells (EC) and the tunica media layer with numerous smooth muscle cells (SMC). A higher power (Figure 8E) shows EC with large lysosomal bodies (arrowheads), irregular and thick basement membrane (short arrows) and the concentric rings of smooth muscle cells (SMC). Interspersed scant pyknotic nuclei are identified in relation with smooth muscle cells (long arrows). A smaller arteriole (Figure 8F) shows a hyperplastic endothelium (EC) with a reduction of the lumen (L), marked thickening of the endothelial basement membranes (arrowheads) and extensive perivascular areas of cell debri, vacuolization of the neuropil (VAC) and abnormal large axons (A). In Figure 8G, EC's are resting on an irregular basement membrane (arrowheads). Variations in the thickness of the basement membrane are significant (Figure 8H, arrowheads).In the same vessel, another feature includes the apparent penetration

of a mononuclear luminal cell (MC) through the endothelium (Figure 8I). The nucleus elongates and indents the basement membrane (short arrow). Notice the close apposition of the mononuclear and the endothelial cell (Figure 8I, long arrows and Figure 8J). Four punctate junction structures are seen between the endothelial and the mononuclear cell (short arrows). A close-up of the basement membrane on the abluminal side of the EC shows a poor definition of the BM limits (Figure 8K arrowheads). The endothelial cell shows a large lysosomal body(*). In figure 8L a 22 nm particle (short arrow) is seen in the endothelial cell cytoplasm close to the basement membrane. There are abundant pinocytic vesicles in the EC cytoplasm (long arrows).

Nanosize particles could be seen in the endothelial cell cytoplasm close to the basement membranes and abundant caveolar activity was present in endothelial cells of MC children (Figure 8L) and strikingly absent in controls. Nanosize PM was seen in RBC, endothelial cell mitochondria, basement membranes and abnormal mitochondria (Figures 9A, 9B, 9C, 9D, 9E). Common observations between RBC and the endothelial cell cytoplasm was the presence of linear accumulation of nanosize particles (Figures 9G, 9H).

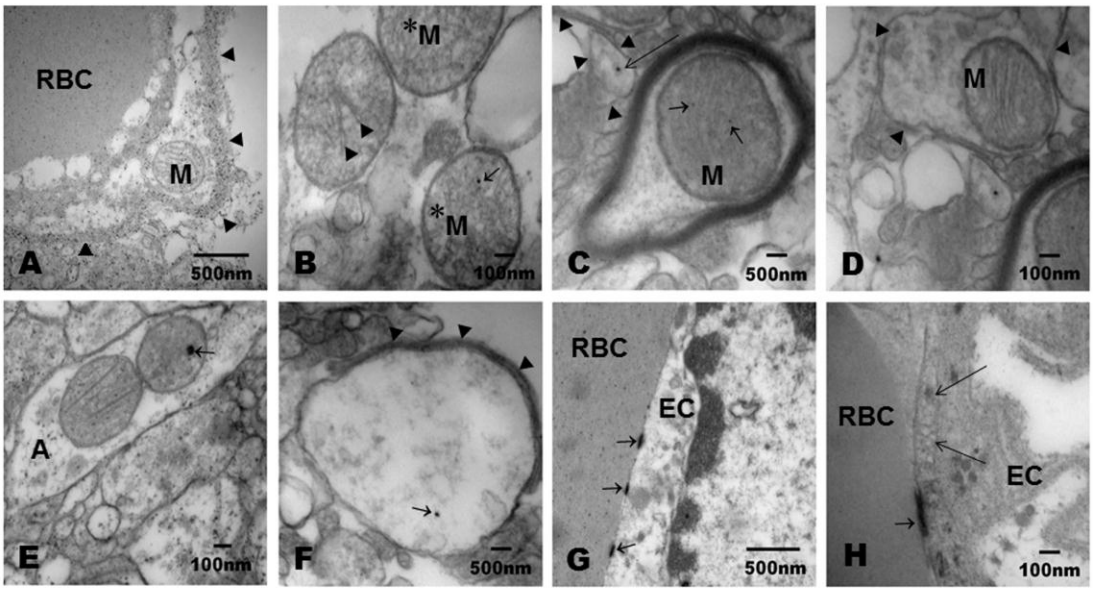

Figure 9. Localization of nanosize particles in the white matter. Figure 9A illustrates nanosize particles in the RBC, an endothelial cell mitochondria (M) and the basement membrane (arrowheads). Particles in the range of 20-38nm are seen in abnormal mitochondria (M) with a few cristae (arrowheads) or no cristae (*)(Figure 9B). An intact mitochondria displaying a couple of particles (short arrows) is seen within a myelinated axon (Figure 9C). In contrast, a poorly preserved dendrite (arrowheads) displays a larger particle measuring 40 nm (long arrow). In an adjacent area (Figure 9D), a poorly preserved unmyelinated axon (arrowheads) shows a mitochondria with no particles. Poorly preserved unmyelinated axons show mitochondria with intact cristae and one single particle 30 nm in diameter (Figure 9E, short arrow). A degenerating myelinated axon with remnants of myelin (arrowheads) shows one single nanosize particle (short arrow)(Figure 9F). A common observation between RBC and the endothelial cell cytoplasm is the presence of linear accumulation of nanosize particles (short arrows) (Figures 9G, 9H). In Figure 9H, a common finding in MC subjects: significant caveolar EC activity (long arrows).

4. DISCUSSION

Vascular and perivascular damage in the prefrontal white matter is a major feature of young Mexico City residents exposed to concentrations of fine particulate matter and ozone above the current USA standards. Major findings including abnormal TJs in endothelial cells, leaking of capillaries, abnormal cerebrovascular basement membranes, and patchy absence of the perivascular glial sheet are likely compromising the integrity of the neurovascular unit. Tight junctions, a critical component of the NVU were abnormal in MC compared to control dogs, and white matter perivascular damage was significantly worse in MC *healthy* dogs.

The potential consequences of this evolving neurovascular unit pathology in urban children and dogs are highly relevant and pivotal to the pathogenesis of vascular-based neurodegenerative disorders like Alzheimer's disease (Zlokovic, 2008; Lo and Rosenberg, 2009; Wardlaw et al., 2013; Winkler et al., 2014; Garwood et al., 2014; Weinl et al., 2015; Elahy et al., 2015; Qosa et al., 2015; Keaney and Campbell, 2015; Tietz and Engelhardt, 2015).

Dysfunction of the NVU in childhood can ultimately lead to devastating short and long term consequences including dysregulation of cerebral blood flow, focal vascular insufficiency, innate immunity dysregulation, neuroinflammation, microstructural altered properties of major fiber tracts and regional volumes of white matter, alterations in ABC efflux transporters expression and/or activity, failure of elimination of interstitial fluid from white matter, vascular deposition of amyloid-β and failure in the flow along pericapillary basement membranes to supply nutrients to the neuropil and equally important, to drain out waste products and soluble metabolites (Weller et al., 2009, 2015; Lo and Rosenberg, 2009; Mathiisen et al., 2010; Hawkes et al., 2014; Keaney and Campbell, 2015; Qosa et al., 2015; Tietz and Engelhardt, 2015; Brickman et al., 2015; Sweeney et al., 2015).The crosstalk between TJ and adherens junctions to maintain barrier integrity is likely to be disrupted, altering CNS homeostasis (Tietz and Engelhardt, 2015; Weinl et al., 2015;Keaney and Campbell,2015).

There are numerous studies recognizing cerebrovascular contributions to neurodegenerative diseases with both neurovascular and neurometabolic uncoupling playing a role in age-related neuropathologies in close association with cognitive decline (Brickman et al., 2015; Lourenco et al., 2015;Haight et al., 2015;Lai et al., 2015).The statement by Lo and Rosenberg (2009) that *sick vessels may generally lead to sick neurons* is of great concern in a developing brain. In the complex scenario of lifetime multiple air pollutant exposures, both the ones we usually measure and the ones we do not, we have plenty of evidence that particulate matter in the nanosize range can induce endothelial damage (Ucciferrini et al., 2014; Alinovi et al., 2015;Bayat et al., 2015; Spigoni et al., 2015;Meng et al., 2015). Nanoparticle exposure is associated to systemic immune responses (Thompson et al., 2014) and endothelial heterogeneity in response to exogenous stimuli, particle potency and composition, sources and the particle content of metals and

endotoxin are key in the evaluation of endothelial damage and inflammatory responses and the severity of oxidative stress (Karthikeyan et al., 2013; Alinovi et al., 2015). Metals are a key component of particles and Mexico City children have high concentrations in the frontal cortex of manganese, nickel and chromium parallel to high expression of COX2, IL1β and TGF-β1 indicating neuroinflammation (Calderón-Garcidueñas et al., 2012a, 2013a,b). IL1β, a major microglial pro-inflammatory cytokine has proven to be an early marker of air pollution exposure in MC children's brains (Calderón-Garcidueñas et al., 2008a), and its role in BBB disruption through downregulation of Sonic hedgehog (SHH) in astrocytes along increased production of pro-inflammatory chemokines including CCL2, CCL20 and CXCL2 are critical for BBB disruption and neuroinflammation (Wang et al., 2014). Up-regulation of TGF-β1 is a common finding in frontal cortex of MC children (Calderón-Garcidueñas et al., 2012a) and chronic production of TGF-β1 in transgenic mice has been associated with AD-like microvascular degeneration (Wyss-Coray et al., 2000).

Both endothelial cell injury and dysfunction are considered early events in air pollution-associated effects and the major marker of endothelial dysfunction: endothelin -1 is quickly produced in response to the combination of particulate matter and ozone (Thomson et al., 2005; Calderón-Garcidueñas et al., 2007, 2008c; Finch and Conklin, 2015). Endothelin-1 is a 21 amino acid peptide with potent vasoconstrictor properties. Vasoconstriction is a potential contributor to cerebral hemodynamic impairment in urban children that can be included in the context of systemic inflammation, vasospasm and induction of focal ischemia (Eisenhut, 2014; Murray et al., 2014; Lei et al., 2015; Nguemeni et al., 2015). ET-1 overexpressing astrocytic cells showed amyloid secretion after a hypoxic/ischemia insult, suggesting astrocytic ET-1 contributes to dementia associated with ischemic stroke (Hung et al., 2015).

Since the major factor determining the impact of neural antibodies is the integrity of the blood-brain-barrier (Diamond et al., 2014; Levin et al., 2010), the autoimmune TJs and neural components seen in MC children potentially add to the ongoing neurovascular unit damage. Complicating the white matter damage scenario is the issue of impaired drainage of interstitial fluid (Laman and Weller, 2013; Weller et al., 2015). MC children have white matter abnormalities on magnetic resonance imaging (MRI) including white matter hyperintensities (WMH) and visible perivascular spaces (PVS) (Calderón-Garcidueñas et al., 2011b, 2012b) and although there is very effective lymphatic drainage for fluid and solutes along restricted pathways in the basement membranes of cerebral capillaries and arteries in young individuals we fully expect lymphatic drainage of the brain is impaired in MC subjects particularly in Apolipoprotein ε4 carriers (Weller et al., 2015). Weller et al., strongly suggest that deposition of proteins in the lymphatic drainage pathways in the walls of cerebral arteries relates to vascular pathology, including cerebral amyloid angiopathy and protein elimination failure angiopathy. In addition, the presence of abnormal proteins, including Aβ in the walls of capillaries and arteries in Mexico City teens and young adults (Calderón-Garcidueñas et al., 2012a, 2013a) may suggests that Aβ is deposited in the pathways by which interstitial fluid drains from the brain as described with great detail by Hawkes et al., (2014). The contribution of the neuropil pathology including the perivascular axonal and dendritic findings cannot be ignored given the strong evidence of the key role of cerebral small vessel vasculopathy to the pathogenesis of Alzheimer's disease (Edwards et al., 2015) and the work of Maillard et al., (2011) showing that WMHs and their penumbra vary in severity and together span a continuous spectrum of white matter injury that worsens with time. Promjunyakul et al., (2015) measured cerebral blood flow (CBF) surrounding WMHs to identify *'WM at risk'*. They concluded CBF penumbra involves

surrounding WMHs, which is associated with future WMH expansion. Prefrontal WMH's are seen in approximately 50% of seemingly healthy Mexico City children and young dogs (Calderón-Garcidueñas et al., 2008b), so the issue is a serious one, potentially affecting around 4 million children in MC alone.

The unfortunate combination of white matter hyperintensities, amyloid β and factors playing a role in modifying cerebral autoregulation in Mexico City children account for vascular risk factors for the development of AD (Calderón-Garcidueñas et al., 2012b, 2013a, 2015a).The white matter damage we are describing in this work could be directly related to two important findings in Mexico City children: 1. The presence of predominantly frontal white matter hyperintensities (WMH) in MC children and their relationship with the complex modulation of cytokines and chemokines and cognitive correlates (Calderón-Garcidueñas et al., 2012b). 2. The statistically significant reduction of the NAA/Cr ratio in the right frontal white matter and decrements on attention, short-term memory, and below-average scores in Verbal and Full Scale IQ (>10 points) in APOE 4 v APOE 3 children (Calderón-Garcidueñas et al., 2015b). Interestingly, young dogs with frontal WMH expand their lesions with time in a strong association with arteriolar pathology (Calderón-Garcidueñas et al., 2008b).The issue of WMH in MC children is very important because white matter microstructure alterations in childhood will result in changes in fluid intelligence later in life (Ritchie et al., 2015). In fact, we are seeing fluid intelligence/working memory changes in elementary school children, teens and in young college students (Calderón-Garcidueñas et al., 2008b, 2015b and unpublished work on progress with Dr. Randall Engle at Georgia Tech). Moreover, WMH relate to cognitive and functional impairment (Prins and Scheltens, 2015).

At the core of the matter is the complex interaction between abnormal tight junctions, BBB dysfunction, small vessel cerebrovascular disease, abnormal cerebrovascular basement membranes, altered cerebral autoregulation, high production of ET-1, nanoparticles damaging endothelial cells, autoimmunity to tight junction and neural proteins, neuroinflammation and lifestyle and vascular risk factors at play in Mexican youth. Of particular concern is childhood obesity and overweight problems with poor diets and high consumption of high fructose sodas. We are observing 11 year old normal weight MC children with 12 h fasting hyperleptinemia related to $PM_{2.5}$ exposures, altered appetite-regulating peptides, and increases in ET-1 (Calderón-Garcidueñas et al., 2015e). These changes could signal the future trajectory of urban children towards the development of insulin resistance, obesity, type II diabetes, addiction-like behavior, cognitive impairment and Alzheimer's disease. Maternal obesity is also in the picture, since the risk for AD will be associated with sustained high-fat diet during gestation and lactation periods, as shown in a mouse model (Hawkes et al., 2015). Using a mouse model of maternal obesity, Hawkes et al found that exposure to a high-fat diet in the fetus and the early neonatal period induced changes in multiple components of the neurovascular unit, including a down-regulation in collagen IV, fibronectin and apolipoprotein E, an up-regulation in markers of astrocytes and perivascular macrophages and altered blood vessel morphology in the brains of adult mice. Interestingly, sustained high-fat diet over the entire lifespan resulted in additional decreases in levels of pericytes and impaired perivascular clearance of Aβ from the brain. These results are very relevant to human populations and support a critical role for early dietary influence on the brain vasculature across the lifespan, with consequences for the developing brain and later cerebrovascular and neurodegenerative diseases (Hawkes et al., 2015).

Two other potential consequences of the NVU pathology are worth commenting in the scenario of children living in polluted environments. The first one is nicely discussed by Licht and Keshet (2015) and pertains to the key issue relating blood vessels to stem cell niches in the brain. The sub-ventricular zone and the hippocampus are the two major neurogenic niches and stem cells are physically associated with blood vessels. Thus, our expectations will include an alteration of the NVU components in these two target areas in highly exposed children. Parenthetically, MC children of the same age as the children in this study show significant low NAA/Cr hippocampal ratios, but not yet robust markers of hippocampal inflammation (IL1β and COX2) (Calderón-Garcidueñas et al., 2008a, 2015c).The second issue has been discussed by several authors including Sweeney et al., and Poggessi et al., 2015 and deals with a pressing need: if indeed the NVU pathology is one key factor in the development of AD then early identification of NVU cell-specific responses including endothelial dysfunction circulating biomarkers ought to be explored in highly exposed children. In this regard, the use of non-invasive techniques to study the NVU integrity are a must, since we are dealing with clinically healthy children. Arterial spin labeling (ASL) a non-invasive MRI technique to measure cerebral blood flow (CBF) could be a useful tool (Grade et al., 2015),while diffusion tensor imaging focusing on diffusivity measures could be used to assess white matter integrity (Nir et al., 2013) along with characterizing major global WM network properties (Fischer et al., 2015). Cerebrospinal fluid markers of NVU dysfunction are critical to study in exposed paediatric populations and a useful source of CSF samples are those labelled as normal in the course of exploratory studies, i.e., work-up for CNS leukaemia involvement (Calderón-Garcidueñas et al., 2015a). Sweeney et al., (2015) have a table depicting CSF markers of BBB breakdown, vascular cells and astrocytes that can be applicable to children's samples from low versus highly polluted places.

4.1 Limitations, perspectives, and future directions

We acknowledge our main limitations include the relatively small group of dogs with optimal EM samples, the lack of optimal preservation of human frontal tissues due to the time between the death of the subjects and the processing of samples, the need to quantitate at a molecular level the mRNA and protein levels of the integral TJs proteins and the flow cytometry analysis of endothelial TJs proteins, inflammatory cytokines and adhesion molecules (Elahy et al., 2015).

Taken together, findings summarized in this work lend strong support to the notion that key components of the neurovascular unit are compromised in highly exposed Mexico City children and young dogs. Advancing from the state of 'guilt by association' in terms of air pollution components and their specific role on the brain impact we are describing, to identification of specific factors altering the NVU is exposed children are critical research areas. Preceding this paramount undertaking, however, further characterization of the biomarkers of neurovascular dysfunction might prove instrumental. Future research needs to address fundamental questions: how early are the white matter changes in the overall MC pediatric population? Are we able to pick up the differences between MC and controls in terms of DTI diffusivity? How early? Are APOE4 carriers different from APOE 3 from early childhood in terms of NVU damage markers? What is the impact of the lifestyle factors in the developing of NVU dysfunction? Are overweight and obese children at higher risk? Or perhaps normal weight children with hyperleptinemia are at high risk as well?

Independently of issues concerning the impact of air pollutants and what specific air pollutants are responsible within the complexity of the atmospheric chemistry and the microenvironments of each subject, there is a pronounced need to identify molecular, structural and functional

phenotypes of children and teens associated with cognition deficits and neurodegenerative features because intervention to protect them is a must. Reliable neurovascular dysfunction biomarkers are essential for early detection of subjects at risk and intervention and to evaluate the effectiveness of early neuroprotection (Sweeney et al., 2015).

In the broad sense, current knowledge should allow us the opportunity to intervene in young urban populations, especially because we have enough evidence that multidimensional interventions are useful and because we cannot ignore the 138% increased risk of AD per increase of 4.34 μg/m3 in $PM_{2.5}$ in the Jung et al., (2015) work suggesting long-term exposure to O_3 and $PM_{2.5}$ is associated with increased the AD risk.

Everybody talks about the enormous health, family, social, and economic burden of Alzheimer's disease, why then ignore the fact that air pollution is likely playing a key role, along with lifestyle and genetic factors and that children's detrimental brain effects have potential serious consequences in the short and long term. There is no support for preventive research. Why?

References

Aiken AC, Salcedo D, Cubison MJ, Huffman JA, DeCarlo PF, Ulbrich IM, Docherty KS, Sueper D, Kimmel JR, Worsnop DR, Trimborn A, Northway M, Stone EA, Schauer JJ, Volkamer RM, Fortner E, de Foy B, Wang J, Laskin A, Shutthanandan V, Zheng J, Zhang R, Gaffney J, Marley NA, Paredes-Miranda G, Arnott WP, Molina LT, Sosa G, Jimenez, JL. Mexico City aerosol analysis during MILAGRO using high resolution aerosol mass spectrometry at the urban supersite (T0) – Part 1: Fine particle composition and organic source apportionment. Atmos Chem Phys 2009; 9; 6633–6653

Alinovi R, Goldoni M, Pinelli S, Campanini M, Aliatis I, Bersani D, Lottici PP, Iavicoli S, Petyx M, Mozzoni P, Mutti A. Oxidative and pro-inflammatory effects of cobalt and titanium oxide nanoparticles on aortic and venous endothelial cells. Toxicol in Vitro 2015; 29:426-437 doi: 10.1016/j.tiv.2014.12.007.

Alonso E, Martínez W, Rubio JC, Velasco F, Chávez HL, Ávalos M, Lara C, Cervantes E. Calidad del aire en cuatro ciudades de Michoacán, México: Su efecto sobre materiales de construcción. Revista de la Construcción 2007; 6:66-74

Bauer HC, Krizbai IA, Bauer H, Traweger A. “You shall not pass”-tight junctions of the blood brain barrier. Frontiers Neuroscience 8:392 doi: 10.3389/fnins.2014.00392.

Bayat N, Lopes VR, Schölermann J, Jensen LD, Cristobal S. Vascular toxicity of ultra-small TiO2 nanoparticles and single walled carbon nanotubes and in vivo. Biomaterials 2015; 63:1-13. doi: 10.1016/j.biomaterials.2015.05.044.

Bergin IL, Witzmann FA. Nanoparticle toxicity by the gastrointestinal route: evidence and knowledge gaps. Int J Biomed Nanosci Nanotechnol 2013; 3: 1-2. doi: 10.1504/IJBNN.2013.054515.

Bravo-Alvarez H, Torres-Jardón R. Air pollution levels and trends in the México City metropolitan area." Chapter 6. In: Urban Air Pollution and Forest: Resources at Risk in the Mexico City Air (M. F. Basin, L. de Bauer, and T. Hernández, eds.) Vol. 156:121-159. Ecological Studies. Springer-Verlag. New York. 2002

Brickman AM, Gúzman VA, Gonzalez-Castellon M, Razlighi Q, Gu Y, Narkhede A, Janicki S, Ichise M, Stern Y, Manly JJ, Schupf N, Marshall RS. Cerebral autoregulation, beta-amyloid and white matter hyperintensities are interrelated. Neurosci Lett 2015; 592:54-58

Cabezas R, Avila M, González J, El-Bachá RS, Báez E, García-Segura LM, Coronel JC, Capani F, Cardona-Gómez GP, Barreto GE. Astrocytic modulation of blood brain barrier: perspectives on Parkinson's disease. Front Cell Neurosci 2014; 8:211. doi: 10.3389/fncel.2014.0021

Calderón-Garcidueñas L, Valencia-Salazar G, Rodriguez-Alcaraz A, Gambling TM, Garcia R, Osnaya N, Villarreal-Calderón A, Devlin RB, Carson JL. Ultrastructural nasal pathology in children chronically and sequentially exposed to air pollutants. Am J Respir Cell Mol Biol 2001; 24: 132-138.

Calderón-Garcidueñas L, Azzarelli B, Acuña H, Garcia R, Gambling TM, Monroy S, Tizapantzi MR, Carson JL, Villarreal-Calderon A, Rewcastle B. Air pollution and brain damage. Toxicol Pathol 2002; 30: 373-389

Calderón-Garcidueñas L, Maronpot R R, Torres-Jardón R, Henríquez-Roldán C, Schoonhoven R, Acuña-Ayala H, Villarreal-Calderón A, Nakamura J, Fernando R, Reed W, Azzarelli B,

Swenberg JA. DNA damage in nasal and brain tissues of canines exposed to air pollutants is associated with evidence of chronic brain inflammation and neurodegeneration. Toxicol Pathol 2003; 31: 524-538

Calderón-Garcidueñas L, Vincent R, Mora-Tiscareño A, Franco-Lira M, Henríquez-Roldán C, Barragán-Mejía G, Garrido-García L, Camacho-Reyes L, Valencia-Salazar G, Paredes R, Romero L, Osnaya H, Villarreal-Calderón R, Torres-Jardón R, Hazucha MJ, Reed W. Elevated plasma endothelin-1 and pulmonary arterial pressure in children exposed to air pollution. Environ Health Perspect 2007; 115: 1248-1253

Calderón-Garcidueñas L, Solt A C, Henríquez-Roldán C, Torres-Jardón R, Nuse B, Herritt L, Villarreal-Calderón R, Osnaya N, Stone I, García R, Brooks D M, González-Maciel A, Reynoso-Robles R, Delgado-Chávez R, Reed W. Long-term air pollution exposure is associated with neuroinflammation, an altered innate immune response, disruption of the blood-brain-barrier, ultrafine particulate deposition, and accumulation of amyloid beta-42 and alpha-synuclein in children and young adults. Toxicol Pathol 2008a; 36: 289-310

Calderón-Garcidueñas L, Mora-Tiscareño A, Ontiveros E, Gómez-Garza G, Barragán-Mejía G, Broadway J, Chapman S, Valencia-Salazar G, Jewells V, Maronpot RR, Henríquez-Roldán C, Pérez-Guillé B, Torres-Jardón R, Herrit L, Brooks D, Osnaya-Brizuela N, Monroy ME, González-Maciel A, Reynoso-Robles R, Villarreal-Calderon R, Solt AC, Engle RW. Air pollution, cognitive deficits and brain abnormalities: A pilot study with children and dogs. Brain and Cognition 2008b; 68: 117-127

Calderón-Garcidueñas L, Villarreal-Calderon R, Valencia-Salazar G, Henríquez-Roldán C, Gutiérrez-Castrellón P, Torres-Jardón R, Osnaya-Brizuela N, Romero L, Torres-Jardón R, Solt

A, Reed W. Systemic inflammation, endothelial dysfunction, and activation in clinically healthy children exposed to air pollutants. Inhal Toxicol 2008c; 20: 499-506

Calderón-Garcidueñas L, Mora-Tiscareño A, Gómez-Garza G, Carrasco-Portugal M del C, Pérez-Guillé B, Flores-Murrieta FJ, Pérez-Guillé G, Juarez-Olguin H, Monroy ME, Monroy S, González-Maciel A, Reynoso-Robles R, Villarreal-Calderón R, Patel SA, Kumarathasan P, Vincent R, Henríquez-Roldán C, Torres-Jardón R, Maronpot R. Effects of a cyclooxygenase 2 preferential inhibitor in young healthy dogs exposed to air pollution: a pilot study. Toxicol Pathol 2009a; 37: 644-660

Calderón-Garcidueñas L, Macías-Parra M, Hoffmann HJ, Valencia-Salazar G, Henríquez-Roldán C, Monte OC, Barragán-Mejía G, Villarreal-Calderon R, Romero L, Granada-Macías M, Torres-Jardón R, Medina-Cortina H, Maronpot RR. Immunotoxicity and Environment: Immunodysregulation and Systemic Inflammation in Children. Toxicol Pathol 2009b; 37:161-169

Calderón-Garcidueñas L, Franco-Lira M, Henríquez-Roldán C, González-Maciel A, Reynoso-Robles R, Villarreal-Calderon R, Herritt L, Brooks D, Keefe S, Palacios- Moreno J, Villarreal-Calderon R, Torres-Jardón R, Medina-Cortina H, Delgado-Chávez R, Aiello-Mora M, Maronpot RR, Doty RL. Urban air pollution: influences on olfactory function and pathology in exposed children and young adults. Exp Toxicol Pathol 2010; 62: 91-102

Calderón-Garcidueñas L, D'Angiulli A, Kulesza R J, Torres-Jardón R, Osnaya N, Romero L, Keefe S, Herritt L, Brooks D M, Avila-Ramirez J, Delgado-Chávez R, Medina-Cortina H, González-González LO. Air pollution is associated with brainstem auditory nuclei pathology and delayed brainstem auditory evoked potentials. Int J Dev Neurosci 2011a*;* 29:365-375

Calderón-Garcidueñas L, Engle R, Mora-Tiscareño A, Styner M, Gómez-Garza G, Zhu H, Jewells V, Torres-Jardón R, Romero L, Monroy-Acosta ME, Bryant C, González-González LO, Medina-Cortina H, D'Angiulli A. Exposure to severe urban pollution influences cognitive outcomes, brain volume and systemic inflammation in clinically healthy children. Brain Cognition 2011b; 77: 345-355

Calderón-Garcidueñas L, Kavanaugh M, Block M L, D'Angiulli A, Delgado-Chávez R, Torres-Jardón R, González-Maciel A, Reynoso-Robles R, Osnaya N, Villarreal-Calderon R, Guo R, Hua Z, Zhu H, Perry G, Diaz P. Neuroinflammation, hyperphosphorilated tau, diffuse amyloid plaques and down- regulation of the cellular prion protein in air pollution exposed children and adults. J Alzheimer Dis 2012a; 28: 93-107

Calderón-Garcidueñas L, Mora-Tiscareño A, Styner M, Gómez-Garza G, Zhu H, Torres-Jardón R, Carlos E, Solorio-López E, Medina-Cortina H, Kavanaugh M, D'Angiulli A. White matter hyperintensities, systemic inflammation, brain growth, and cognitive functions in children exposed to air pollution. J Alzheimers Dis 2012b; 31: 183-191

Calderón-Garcidueñas L, Franco-Lira M, Mora-Tiscareño A, Medina-Cortina H, Torres-Jardón R, Kavanaugh M. Early Alzheimer's and Parkinson's disease pathology in urban children: Friend versus Foe responses- It is time to face the evidence. Biomed Res Int doi: 10.1155/2013/161687. 2013a

Calderón-Garcidueñas L, Serrano-Sierra A, Torres-Jardón R, Zhu H, Yuan Y, Smith D, Delgado-Chávez R, Cross JV, Medina-Cortina H, Kavanaugh M, Guilarte TR. The impact of environmental metals in young urbanites' brains. Exp Toxicol Pathol 2013b; 65: 503-511

Calderón-Garcidueñas L, Franco-Lira M, Rodríguez-Díaz J, Chao C, Thompson C, Mukherjee PS, Perry G. CSF biomarkers: low amyloid-β $_{1-42}$ and BDNF and high IFN γ differentiate children exposed to Mexico City high air pollution v controls. Alzheimer's Disease Uncertainties. J Alzheimer Disease and Parkinsonism 2015a, 5:2 http://dx.doi.org/10.4172/2161-0460.1000189

Calderón-Garcidueñas L, Mora-Tiscareño A, Franco-Lira M, Zhu H, Lu Z, Solorio E, Torres-Jardón R, D'Angiulli A. Decreases in Short Term Memory, IQ, and Altered Brain Metabolic Ratios in Urban Apolipoprotein ε4 Children Exposed to Air Pollution. J Alzheimers Dis. 2015b;45:757-770

Calderón-Garcidueñas L, Mora-Tiscareño A, Melo- Sánchez G, Rodríguez-Díaz J, Torres-Jardón R, Styner M, Mukherjee PS, Lin W, Jewells V. A critical proton MR spectroscopy marker of Alzheimer early neurodegenerative change: low hippocampal NAA/Cr ratio impacts APOE 4 Mexico City children and their parents. J Alzheimers Dis. 2015c

Calderón-Garcidueñas L, Vojdani A, Blaurock-Busch E, Busch I, Friedle A, Franco-Lira M, Sarathi-Mukherjee P, Park SB, Torres-Jardón R, D'Angiulli A. Air pollution and children: neural and tight junction antibodies and combustion metals, the role of barrier breakdown and brain immunity in neurodegeneration. J Alzheimer's Disease 2015d;43:1039-1058

Calderón-Garcidueñas L, Franco-Lira M, D'Angiulli A, Rodriguez-Diaz J, Blaurock-Busch E, Busch I, Chao CK, Thompson C, Mukherjee PS, Torres-Jardón R, Perry G. Mexico City normal weight children exposed to High concentrations of ambient PM2.5 show High blood leptin and endothelin-1, vitamin D deficiency, and food reward hormone dysregulation versus low pollution controls. Relevance for obesity and Alzheimer disease. Env Res 2015e; 140:579-592

Carson JL, Brighton LE, Collier A M, Bromberg PA. Correlative ultrastructural investigations of airway epithelium following experimental exposure to defined air pollutants and lifestyle exposure to tobacco smoke. Inhal Toxicol 2013; 25: 134-140

Castejón OJ. Ultrastructural pathology of endothelial tight junctions in human brain edema. Folia Neuropath 2012; 50:118-129

Castejón OJ. Ultrastructural alterations of human cortical capillary basement membrane in human brain oedema. Folia Neuropath 2014; 52: 10-21

Diamond B, Honig G, Mader S, Brimberg L, Volpe BT. Brain-reactive antibodies and disease. Ann Rev Immunol 2014; 31: 345-385

Edwards JD, Ramírez J, Black SE. Unraveling the potential co-contributors of cerebral small vessel vasculopathy to the pathogenesis of Alzheimer's dementia. Alzheimers Res Ther 2015; 7(1):49. doi: 10.1186/s13195-015-0133-2

Elahy M, Jackaman C, Mamo JC, Lam V, Dhaliwal SS, Giles C, Nelson D, Takechi R. Blood-brain-barrier dysfunction developed during normal aging is associated with inflammation and loss of tight junctions but not with leukocyte recruitment. Immun Ageing 2015;12:2. doi: 10.1186/s12979-015-0029-9.

Eisenhut M. Vasospasm in cerebral inflammation. Int J Inflam 2014 doi: 10.1155/2014/509707.

Finch J, Conklin DJ. Air pollution-induced vascular dysfunction: Potential role of endothelin-1 (ET-1) system. Cardiovasc Toxicol 2015

Fischer FU, Wolf D, Scheurich A, Fellgiebel A, Alzheimer's Disease Neuroimaging Initiative.Altered whole-brain white matter networks in preclinical Alzheimer's disease. Neuroimage Clin 2015; 8:660-666 doi: 10.1016/j.nicl.2015.06.007

Garwood CJ, Simpson JE, Al Mashhadi S, Axe C, Wilson S, Heath PR, Shaw PJ, Matthews FE, Brayne C, Ince PG, Wharton SB; MRC Cognitive Function and Ageing Study. DNA damage response and senescence in endothelial cells of human cerebral cortex and relation to Alzheimer's neuropathology progression: a population-based study in the Medical Research Council Cognitive Function and Ageing Study (MRC-CFAS) cohort. Neuropathol Appl Neurobiol 2014; 40:802-814

Gehr P, Clift M J, Brandenberger C, Lehmann A, Herzog F, Rothen-Rutishauser B. Endocytosis of environmental and engineered micro-and nanosized particles. Compar Physiol 2011; 1: 1159-1174

Grade M, Hernández-Tamames JA, Pizzini FB, Achten E, Golay X, Smits M. A neuroradiologist's guide to arterial spin labeling MRI in clinical practice. Neuroradiology 2015 Sep 9

Haight TJ, Bryan RN, Erus G, Davatzikos C, Jacobs DR, D'Esposito M, Lewis CE, Launer LJ. Vascular risk factors, cerebrovascular reactivity and the default-mode brain network. Neuroimage 2015; 115:7-16 doi: 10.1016/j.neuroimage.2015.04.039.

Harkema JR, Carey SA, Wagner JG. The nose revisited: a brief review of the comparative structure, function, and toxicologic pathology of the nasal epithelium. Toxicol Pathol 2006; 34: 252-269

Haseloff RF**,** Dithmer S**,** Winkler L**,** Wolburg H**,** Blasig IE**.** Transmembrane proteins of the tight junctions at the blood-brain barrier: structural and functional aspects. Semin Cell Dev Biol 2015; 38:16-25 doi: 10.1016/j.semcdb.2014.11.004

Hawkes CA, Jayakody N, Johnston DA, Bechmann I, Carare RO. Failure of perivascular drainage of β-amyloid in cerebral amyloid angiopathy. Brain Pathol 2014; 24:396-403

Hawkes CA, Gentleman SM, Nicoll JA, Carare RO. Prenatal high-fat diet alters the cerebrovasculature and clearance of β-amyloid in adult offspring. J Pathol 2015; 235:619-631

Hung VK, Yeung PK, Lai AK, Ho MC, Chan KC, Wu EX, Chung SS, Cheung CW, Chung SK. Selective astrocytic endothelin-1 overexpression contributes to dementia associated with ischemic stroke by exaggerating astrocyte-derived amyloid secretion. J Cereb Blood Flow Metab 2015; doi: 10.1038/jcbfm.2015.109.

Iadecola C. Neurovascular regulation in the normal brain and in Alzheimer's disease. Nat Rev Neurosci 2004; 5: 347-360

Jung CR, Lin YT, Hwang BF. Ozone, particulate matter and newly diagnosed Alzheimer's disease: a population-based cohort study in Taiwan. J Alzheimers Dis 2015; 44: 573-584

Kamat PK, Swarnkar S, Rai S, Kumar V, Tyagi N. Astrocyte mediated MMP-9 activation in the synapse dysfunction: An implication in Alzheimer disease. Ther Targets Neurol Dis. 2014;1(1). pii: e243.

Kaplan GG, Hubbard J, Korzenik J, Sands BE, Panaccione R, Ghosh S, Wheeler AJ, Villeneuve PJ. The inflammatory bowel diseases and ambient air pollution: A novel association. Am J Gastroenterol 2010; 105:2412- 2419

Karmakar A, Zhang Q, Zhang Y. Neurotoxicity of nanoscale materials. J Food Drug Anal 2014; 22:147-160

Karthikeyan S, Thomson EM, Kumarathasan P, Guénette J, Rosenblatt D, Chan T, Rideout G, Vincent R. Nitrogen dioxide and ultrafine particles dominate the biological effects of inhaled diesel exhaust treated by a catalyzed diesel particulate filter. Toxicol Sci 2013; 135:437-450

Keaney J, Campbell M. The dynamic blood-brain-barrier. FEBS J. 2015 Aug 16. doi: 10.1111/febs.13412

Lacoste B, Gu C. Control of cerebrovascular patterning by neural activity during postnatal development. Mech Dev 2015, pii: S0925-4773(15)00047-7. doi: 10.1016/j.mod.2015.06.003.

Lai AY, Dorr A, Thomason LA, Koletar MM, Sled JG, Stefanovic B, Mclaurin J. Venular degeneration leads to vascular dysfunction in a transgenic model of Alzheimer's disease. Brain 2015; 138(Pt 4):1046-1058 doi: 10.1093/brain/awv023.

Laman JD, Weller RO. Drainage of cells and soluble antigen from the CNS to regional lymph nodes. J Neuroimmune Pharmacol 2013; 8:840-856

Lecrux C, Hamel E. The neurovascular unit in brain function and disease. Acta Physiol. (Oxf.), 2011; 203: 47–59

Lei Q, Li S, Zheng R, Xu K, Li S. Endothelin-1 expression and alterations of cerebral microcirculation after experimental subarachnoid hemmorrhage. Neuroradiology 2015; 57:63-70

Levin EC, Acharya NK, Han M, Zavareh SB, Sedeyn JC, Venkataraman V, Nagele RG. Brain-reactive autoantibodies are nearly ubiquitous in human sera and may be linked to pathology in the context of blood-brain barrier breakdown. Brain Res 2010; 1345: 221-232

Li CH, Jhan C, Cheng YW, Tsai CH, Liu CW, Lee CC, Chen RM, Shyu MK, Kang JJ. Gold nanoparticles increase endothelial paracellular permeability by altering components of

endothelial tight junctions, and increase blood-brain barrier permeability in mice. Toxicol Sci. 2015 Aug 13. pii: kfv176.

Licht T, Keshet E. The vascular niche in adult neurogenesis. Mech Dev 2015 doi: 10.1016/j.mod.2015.06.001 pii: S0925-4773(15)00045-3

Ljubimova JY, Kleinman MT, Karabalin NM, Inoue S, Konda B, Gangalum P, Markman JL, Ljubimov AV, Black KL. Gene expression changes in rat brain after short and long exposures to particulate matter in Los Angeles basin air. Comparison with human brain tumors. Exp Toxicol Pathol 2013;65:1063-1071

Lo EH, Rosenberg GA. The neurovascular unit in health and disease. Stroke 2009; 40:S2-S3

Lourenco CF, Ledo A, Dias C, Barbosa RM, Laranjinha J. Neurovascular and neurometabolic derailment in aging and Alzheimer's disease. Front Aging Neurosci 2015; 7:103. doi: 10.3389/fnagi.2015.00103.

Love S, Miners JS. White matter hypoperfusion and damage in dementia: post-mortem assessment. Brain Pathol 2015; 25:99-107

Maillard P, Fletcher E, Harvey D, Carmichael O, Reed B, Mungas D, DeCarli C. White matter hyperintensity penumbra. Stroke 2011; 42**;** 1917-1922

Mathiisen TM, Lehre KP, Danbolt NC, Ottersen OP. The perivascular astroglial sheath provides a complete covering of the brain microvessels: an electron microscopic 3D reconstruction. Glia 2010; 58:1094-1103 doi: 10.1002/glia.20990.

Meng N, Han L, Pan X, Su L, Jiang Z, Lin Z, Zhao J, Zhang S, Zhang Y, Zhao B, Miao J. Nano-Mg(OH)2-induced proliferation inhibition and dysfunction of human umbilical vein vascular endothelial cells through caveolin-1-mediated endocytosis. Cell Biol Toxicol 2015; 31:15-27

Molina LT, Madronich SJ, Gaffney JS, Apel E, de Foy B, Fast J, Ferrare R, Herndon S, Jimenez J L, Lamb B, Osornio-Vargas AR, Russell P, Schauer JJ, Stevens PS, Volkamer R, Zavala M. An overview of the MILAGRO 2006 Campaign: Mexico City emissions and their transport and transformation. Atmos Chem Phys 2010; 10: 8697–8760

Morris AWJ, Carare RO, Schreiber S, Hawkes CA. The cerebrovascular basement membrane: role in the clearance of β- amyloid and cerebral amyloid angiopathy. Front Aging Neurosci 2014; doi: 10.3389/fnagi.2014.00251

Múgica V, Torres M, Salinas E, Gutiérrez M, García R. Polycyclic Aromatic Hydrocarbons in the Urban Atmosphere of Mexico City. In: Air Pollution, Vanda Villanyi (Ed.), InTech 2010; 73-97. Available from: http://www.intechopen.com/books/air-pollution/polycyclic-aromatichydrocarbons-in-the-urban-atmosphere-of-mexico-city.

Muir AR, Peter A. Quintuple-layered membrane junctions at terminal bars between endothelial cells. J Cell Biol 1962; 12: 443-448

Murray KN, Girard S, Holmes WM, Parkes LM, Williams SR, Parry-Jones AR, Allan SM. Systemic inflammation impairs tissue reperfusion through endothelin-dependent mechanisms in cerebral ischemia. Stroke 2014; 45:3412-3419

Nir TM, Jahanshad N, Villalon-Reina JE, Toga AW, Jack CR, Weiner MW, Thompson PM, Alzheimer's Disease Neuroimaging Initiative (ADNI). Effectiveness of regional DTI measures

in distinguishing Alzheimer's disease, MCI and normal aging. Neuroimage Clin 2013; July 27;3: 180-195

Nguemeni C, Gomez-Smith M, Jeffers MS, Schuch CP, Corbett D. Time course of neuronal death following endothelin-1 induced focal ischemia in rats. J Neurosci Methods 2015; 242:72-76

Poggesi A, Pasi M, Pescini F, Pantoni L, Inzitari D. Circulating biologic markers of endothelial dysfunction in cerebral small vessel disease: a review. J Cereb Blood Flow Metab 2015 Jun 10. doi: 10.1038/jcbfm.2015.116.

Prins ND, Scheltens P. White matter hyperintensities, cognitive impairment and dementia: an update. Nat Rev Neurol 2015; 11:157-165

Promjunyakul N, Lahna D, Kaye JA, Dodge HH, Erten-Lyons D, Rooney WD, Silbert LC. Characterizing the white matter hyperintensity penumbra with cerebral blood flow measures. Neuroimage Clin 2015; 8:224-229

Querol X, Pey J, Minguillón MC, Pérez N, Alastuey A, Viana M, Moreno T, Bernabé RM, Blanco S, Cárdenas B, Vega E, Sosa G, Escalona S, Ruiz H, Artíñano B. PM speciation and sources in Mexico during the MILAGRO-2006 Campaign. Atmos Chem Phys 2008; 8: 111–128

Qosa H, Miller DS, Pasinelli P, Trotti D. Regulation of ABC efflux transporters at blood-brain barrier in health and neurological disorders. Brain Res. 2015 Jul 15. pii: S0006-8993(15)00530-2. doi: 10.1016/j.brainres.2015.07.005.

Semarnathttp://www.semarnat.gob.mx/archivosanteriores/temas/gestionambiental/calidaddelaire/Documents/ProAire%20Puebla2.pdf

Retama A, Baumgardner D, Raga GB, McMeeking GR, Walker JW. Seasonal and diurnal trends in black carbon properties and co-pollutants in Mexico City. Atmos Chem Phys 2015; 15: 9693–9709

Ritchie SJ, Bastin ME, Tucker-Drob EM, Maniega SM, Engelhardt LE, Cox SR, Royle NA, Gow AJ, Corley J, Pattie A, Taylor AM, Valdés Hernández M del C, Starr JM, Wardlaw JM, Deary IJ. Coupled changes in brain white matter microstructure and fluid intelligence in later life. J Neurosci 2015; 35:8672-8682

Seinfeld JH, Pandis SN. Atmospheric Chemistry and Physics: From Air Pollution to Climate Change, 1st edition, J. Wiley, New York, 1998.

Simard M, Arcuino G, Takano T, Liu QS, Nedergaard M. Signaling at the gliovascular surface. J Neurosci 2003; 23:9254-9262

Spigoni V, Cito M, Alinovi R, Pinelli S, Passeri G, Zavaroni I, Goldoni M, Campanini M, Aliatis I, Mutti A, Bonadonna RC, Dei Cas A. Effects of TiO2 and CO3O4 nanoparticles on circulating angiogenic cells. PLoS One 2015 Mar 24;10(3):e0119310. doi: 10.1371/journal.pone.0119310.

Sharma A, Muresanu D F, Patnaik R, Sharma HS. Size and age-dependent neurotoxicity of engineered metal nanoparticles in rats. Mol Neurobiol 2013; 48: 386-396

Sweeney MD, Sagare AP, Zlokovic BV. Cerebrospinal fluid biomarkers of neurovascular dysfunction in mild dementia and Alzheimer's disease. J Cerebral Blood Flow & Metabolism 2015; 35:1055-1068

Thompson EA, Sayers BC, Glista-Baker EE, Shipkowski KA, Taylor AJ, Bonner JC. Innate immune responses to nanoparticle exposure in the lung. J Environ Immunol Toxicol. 2014; 1:150-156

Thomson EM, Kumarathasan P, Goegan P, Aubin RA, Vincent R. Differential regulation of the lung endothelin system by urban particulate matter and ozone. Toxicol Sci 2005; 88:103–113

Tietz S, Engelhardt B**.** Brain barriers: Crosstalk between complex tight junctions and adherens junctions. J Cell Biol 2015; 209:493-506 doi: 10.1083/jcb.201412147.

Ucciferri N, Collnot EM, Gaiser BK, Tirella A, Stone V, Domenici C, Lehr CM, Ahluwalia A. In vitro toxicological screening of nanoparticles on primary human endothelial cells and the role of flow in modulating cell response. Nanotoxicology 2014; 8:697-708

Van Miert E, Dumont X, Bernard A. CC16 as a marker of lung epithelial hyperpermeability in an acute model of rats exposed to mainstream cigarette smoke. Toxicol Lett 2005; 159: 115-123

Vega E, Eidels S, Ruiz H, López-Veneroni D, Sosa G, Gónzalez E, Gasca J, Mora V, Reyes E, Sánchez-Reyna G, Villaseñor R, Chow JC, Watson JG, Edgerton SA. Particulate air pollution in Mexico City: A detailed view. Aerosol and Air Quality Research 2010; 10:193-211

Villarreal-Calderón A, Acuña H, Villarreal-Calderón J, Garduño M, Henríquez-Roldán CF, Calderón-Garcidueñas L, Valencia-Salazar G. Assessment of physical education time and after-school outdoor time in elementary and middle school students in south Mexico City: the

dilemma between physical fitness and the adverse health effects of outdoor pollutant exposure. Arch Environ Health 2002; 57: 450-460

Wang Y, Jin S, Sonobe Y, Cheng Y, Horiushi H, Parajuli B, Kawanokuchi J, Mizuno T, Takeuchi H, Suzumura A. Interleukin-1β induces blood-brain-barrier disruption by downregulating Sonic hedgehog in astrocytes. PLoS One. 2014 Oct 14;9(10):e110024. doi: 10.1371/journal.pone.0110024.

Wang Z, Tiruppathi C, Minshall RD, Malik AB. Size and dynamics of caveolae studied using nanoparticles in living endothelial cells. ACS Nano 2009; 3:4110-4116

Wardlaw JM, Smith EE, Biessels GH,Cordonnier C, Fazekas F, Frayne R, Lindley RI, O'Brien JT, Barkhof F, Benavente OR, Black SE, Brayne C, Breteler M, Chabriat H, DeCarli C, de Leeuw FE, Doubal F, Duering M, Fox NC, Greenberg S, Hachinski V, Kilimann I, Mok V, van Oostenbrugge R, Pantoni L, Speck O, Stephan BCM, Teipel S, Viswanathan A, Werring D, Chen C, Smith C, van Buchem M, Norrving B,Gorelick PB, Dichgans M, STandards for ReportIng Vascular changes on nEuroimaging (STRIVE v1). Neuroimaging standards for research into small vessel disease and its contribution to ageing and neurodegeneration. Lancet Neurol. 2013;12: 822–838

Weinl C, Castaneda-Vega S, Riehle H, Stritt C, Calaminus C, Wolburg H, Mauel S, Breithaupt A, Gruber AD, Wasylyk B, Olson EN, Adams RH, Pichler BJ, Nordheim A. Endothelial depletion of murine SRF/MRTF provokes intracerebral hemorrhagic stroke. Proc Natl Acad Sci U S A. 2015;112: 9914-9919

Weller RO, Boche D, Nicoll JA. Microvasculature changes and cerebral amyloid angiopathy in Alzheimer's disease and their potential impact on therapy. Acta Neuropath 2009; 118: 87-102

Weller RO, Hawkes CA, Kalaria RN, Werring DJ, Carare RO. White matter changes in dementia: role of impaired drainage of interstitial fluid. Brain Pathol 2015; 25:63-78

Winkler EA, Sagare AP, Zlokovic BV. The pericyte: a forgotten cell type with important implications for Alzheimer's disease? Brain Pathol 2014; 24:371-86. doi: 10.1111/bpa.12152.

Wyss-Coray T, Lin C, Sanan DA, Mucke L, Masliah E. Chronic overproduction of Transforming growth factor β-1 by astrocytes promotes Alzheimer's disease-like microvascular degeneration in transgenic mice. Am J Pathol 2000; 156:139-150

Yu SH, Tang DW, Hsieh HY, Wu WS, Lin BX, Chuang EY, Sung HW, Mi FL. Nanoparticle-induced tight-junction opening for the transport of an anti-angiogenic sulfated polysaccharide across Caco-2 cell monolayers. Acta Biomater 2013; 9: 7449-7459

Zlokovic BV. The blood-brain-barrier in health and chronic neurodegenerative disorders. Neuron 2008; 57:178-201

TABLES

Table 1 Summary of results comparing Mexico City with low air pollution control dogs'

	Controls n:6	Mexico City n:9	p value
Age in years	3.23±0.81 years	3.11±0.67 years	0.95
Gender	3F/3M	5F/4M	NA
White matter percentage damaged area*	0.77±0.46	19.43±2.69	0.002

* Measured in a 60μm^2 area/16 areas from 4 slides 2R/2L

Table 2 Summary of Controls and Mexico City children and teens selected for light and electron microscopy prefrontal samples

CONTROLS AGE	CONTROLS GENDER	CONTROLS APOE
8.2	1	34
17	1	33
13	1	33
7.8	0	33
16	1	34
14	1	33
15	1	33
10	0	33
12.62±3.5 years	6M/2F	2 APOE 3/4
MC AGE	MC GENDER	MC APOE
15	1	44
13	0	34

15	1	44
18	1	44
17	1	33
11	1	33
16	1	33
2	1	33
17	1	33
17	1	33
12	1	33
3	1	33
17	1	33
17	1	33
11	0	33
14	1	33
14	0	33
1	1	33
7	0	33
13	1	33
15	1	33
14	0	33
13	0	33
11	0	33
15	0	33
16	1	33
12.67±4.9 years	18M/8F	4 APOE4

FIGURES

Figures 1 and 2. Box plots for 24-hour $PM_{2.5}$ concentrations at two representative sites of Mexico City Metropolitan Area: Pedregal (residential area) and Xalostoc industrial and high traffic (area) from 1997 to 2014. The dashed lines inside the boxes are the annual average and the continuous lines the 24-hr median. The $PM_{2.5}$ annual mean NAAQS concentration value is represented by the dashed blue line and the $PM_{2.5}$ 24-hr average NAAQS level is shown with the red continuous line. Due that PM $_{2.5}$ data were not available in MCMA until 2004, the PM2.5 trends were approximated using a correlation equation of the $PM_{2.5}/PM_{10}$ ratio for the period 2004-2011 and PM_{10} data measured at each site of the period 1997-2003. PM_{10} and $PM_{2.5}$ data were obtained from the Secretaría del Medio Ambiente del Distrito Federal **(**http://www.aire.df.gob.mx**).**

Figure 3. Average mass and composition of PM coarse (PM_{10}–$PM_{2.5}$), $PM_{2.5}$ and PM_1 at the Instituto Mexicano del Petróleo site (northern Mexico City) during March 2006 (based upon a compilation of Molina et al., 2010, Querol et al., 2008 and Aitken et al., 2009).

Figure 4. Light microscopy assessment using toluidine blue staining in dog's frontal white matter. Unremarkable white matter is characteristic of control dogs (Figure 4A). Virchow-Robin (VR) spaces are free of mononuclear cells, red blood cells or lipid droplets. The neuropil is unremarkable and the myelinated axons (A) vary in size, they are uniformly distributed and they are intact. In contrast, Mexico City dogs exhibit expanded VR spaces with mononuclear cells characterized by large nuclei with increased chromatin condensation (Figure 4B, arrowheads). Scattered through the neuropil, cells with large nuclei and increased chromatin condensation are present (Figure 4B short arrows). Patchy pallor of the neuropil with zones where the myelinated

axons are scanty and alternate with clusters of small myelinated fibers (Figure 4C square) and cells showing prominent chromatin condensation (Figure 4C arrowheads) are common in MC dogs. Small arterioles show thick walls and expanded VR spaces (long arrows). In Figure 4D we observed extensive areas of rarefaction of the neuropil around blood vessels (*). Large perivascular cells have the morphology of macrophages (arrowheads), while clusters of lipid droplets are prominent around blood vessels (long arrows). In Figure 4E, a close up of a typical blood vessel in a young dog showing large accumulation of lipids (arrowheads). Figure 4F shows a postcapillary venule with perivascular lipid accumulation (arrowheads). Distributed throughout the frontal white matter, small blood vessels (Figure 4G) exhibit hyperplastic endothelial cells (arrowheads) reducing their lumen (L). Mononuclear cells are seen attached to the hyperplastic endothelium (long arrow). In the transition between the subcortical white and gray matter (Figure 4H), abnormal small vessels are also present with RBC occupying the perivascular space (arrowheads). Remarkably, neuronal bodies in the transition area have vacuolated cytoplasm (short arrows).

Figure 5. Light microscopy assessment using toluidine blue staining in children's frontal white matter. Control children (Figure 5A) exhibit unremarkable blood vessels, Virchow-Robin (VR) spaces and neuropil. MC children show lipid material accumulation around blood vessels (Figure 5B *) and a significant expansion of the VR space and clusters of perivascular lipids (Figure 5C, short arrows). Scattered small tortuous blood vessels show mononuclear cells (Figure 5D, arrowheads) in the expanded perivascular spaces (*). A few large axons (A) show intraaxonal vacuolation (short arrows) and curled membrane fragments (long arrows). Leaking of lipid material also affects small capillaries (Figure 5E*). A few of the blood vessels architecture is completely lost (Figure 5F). Scattered unidentified cells show clumping of the

chromatin (short arrows).Hyperplastic endothelial cells are also seen (Figure 5G, arrowheads). In the transition between the subcortical white and gray matter, abnormal small vessels are present with amorphous material occupying the intra and perivascular spaces (Figure 5H*).

Figure 6. Electron microscopy of dogs' blood vessels. An abnormal small blood vessel (Figure 6A) with irregular endothelial basement membranes (arrowheads) and an apparently intact perivascular glial sheath (short arrows) shows clusters of lipid material (*). RBC are seen in the perivascular space. Figure 6B shows a capillary vessel with a wide perivascular space (*) occupied by cell fragments (short arrows). Note the significant rarefaction of the neuropil on the right side of the picture (square). Early formation of lipofuscin is seen in pericytes of <3y old dogs (Figure 6C short arrow).Capillaries show irregular luminal endothelial cell (EC) surface with microvilli-like protrusions (long arrow) and a large perivascular space with abundant cellular debri (*). A close up of the lipofuscin formation can be seen in Figure 6D. A lipofuscin granule (*Lf*) with dense osmiophilic content, and one mitochondria with abnormal cristae *(*Figure 6D, short arrow*)* lie in the adjacent cytoplasm. In Figure 6E, a small vessel shows a thick and irregular basement membrane (arrowheads). Scattered capillaries show cells in the position of pericytes and smooth muscle cells with semicircular or circular thickening of vascular walls containing large amounts of amorphous material (Figure 6F *) and smaller areas with amyloid-like fibrils (short arrows). The endothelial cell shows microvilli-like protrusions (long arrow) and there is a white blood cell (WBC) and one RBC occupying the vessel lumen (L). Figure 6G shows helical twist amyloid fibers with a 35-50A repeat(short arrow).A blood vessel with a prominent endothelial cell nucleus (EC) protruding in the lumen is seen in Figure 6H along with RBC.A smooth muscle cell (SMC) cytoplasm display multiple mitochondria (short arrows). An unidentified perivascular structure shows a vacuolated background (*) with cellular fragments

(short arrows). A capillary with an attached white blood cell (WBC) occupies the lumen of the vessel (Figure 6I).

Figure 7. Electron microscopy of dogs' blood vessels. White matter arterioles display layers of smooth muscle cells (SMC)(Figure 7A). Endothelial cells (short arrows) and RBC are seen. In a close-up (Figure 7B), the typical components of a smooth cell cytoplasm are present, bundles of microfilaments (short arrows), elastic microfibrils (arrowheads), dense bodies and mitochondria (long arrows). A close-up of a tight junction between two endothelial cells (EC) is seen in Figure 7C (arrowheads). A significant number of prefrontal white matter capillaries (Figure 7D) in MC dogs are characterized by wide VR spaces and the patchy absence of astrocytic perivascular endfeet (arrowheads). Mononuclear cells (short arrows) occupy the VR space and project cytoplasmic processes towards the capillary wall (long arrows). Patchy areas of neuropil (*) are characterized by the absence of axons and cellular profiles. Figure 7E is a higher power of the square in Fig 7D to focus on tight junctions in endothelial cells. A series of tight junctions (short arrows) between endothelial cells define the limits between cells. A RBC is seen in the lumen of the capillary. A higher power of the TJ's (Figure 7F) illustrates the clear lining of the cleft (white arrowheads) alternating with the presence of osmiophilic granular material obliterating the cleft of the TJs (short arrows). A portion of the RBC is seen in the lumen of the capillary. Higher magnification (150,000 x) shows a TJs intact segment (Figure 7G arrowhead) and the lack of integrity of the TJ's (short arrows). In Figure 7H a TJs (arrowheads) is intact in a control animal (RBC in lumen).

Figure 8. Electron microscopy of children' prefrontal white matter. A prefrontal white matter small blood vessel (Figure 8A) exhibits a typical finding in MC children: accumulation of

lipofuscin (arrowheads) in pericytes. Extensive accumulation of lipofuscin (*Lf*) is a major finding in perivascular cells (Figure 8B). A pericyte is present (arrowheads), along with a RBC occupying the entire vessel lumen. In Figure 8C, an olidendroglial cell (OLIGO) is seen adjacent to a small blood vessel with an undulating basement membrane (arrowheads). Striking arteriolar white matter changes are observed in MC teens (Figure 8D). An arteriole exhibits an irregular and thick basement membrane (short arrows) between the endothelial cells (EC) and the tunica media layer with numerous smooth muscle cells (SMC). A higher power (Figure 8E) shows EC with large lysosomal bodies (arrowheads), irregular and thick basement membrane (short arrows) and the concentric rings of smooth muscle cells (SMC). Interspersed scant pyknotic nuclei are identified in relation with smooth muscle cells (long arrows). A smaller arteriole (Figure 8F) shows a hyperplastic endothelium (EC) with a reduction of the lumen (L), marked thickening of the endothelial basement membranes (arrowheads) and extensive perivascular areas of cell debri, vacuolization of the neuropil (VAC) and abnormal large axons (A). In Figure 8G, EC's are resting on an irregular basement membrane (arrowheads). Variations in the thickness of the basement membrane are significant (Figure 8H, arrowheads).In the same vessel, another feature includes the apparent penetration of a mononuclear luminal cell (MC) through the endothelium (Figure 8I). The nucleus elongates and indents the basement membrane (short arrow). Notice the close apposition of the mononuclear and the endothelial cell (Figure 8I, long arrows and Figure 8J). Four punctate junction structures are seen between the endothelial and the mononuclear cell (short arrows). A close-up of the basement membrane on the abluminal side of the EC shows a poor definition of the BM limits (Figure 8K arrowheads). The endothelial cell shows a large lysosomal body(*). In figure 8L a 22 nm particle (short arrow) is seen in the

endothelial cell cytoplasm close to the basement membrane. There are abundant pinocytic vesicles in the EC cytoplasm (long arrows).

Figure 9. Localization of nanosize particles in the white matter. Figure 9A illustrates nanosize particles in the RBC, an endothelial cell mitochondria (M) and the basement membrane (arrowheads). Particles in the range of 20-38nm are seen in abnormal mitochondria (M) with a few cristae (arrowheads) or no cristae (*)(Figure 9B). An intact mitochondria displaying a couple of particles (short arrows) is seen within a myelinated axon (Figure 9C). In contrast, a poorly preserved dendrite (arrowheads) displays a larger particle measuring 40 nm (long arrow). In an adjacent area (Figure 9D), a poorly preserved unmyelinated axon (arrowheads) shows a mitochondria with no particles. Poorly preserved unmyelinated axons show mitochondria with intact cristae and one single particle 30 nm in diameter (Figure 9E, short arrow). A degenerating myelinated axon with remnants of myelin (arrowheads) shows one single nanosize particle (short arrow)(Figure 9F). A common observation between RBC and the endothelial cell cytoplasm is the presence of linear accumulation of nanosize particles (short arrows) (Figures 9G, 9H). In Figure 9H, a common finding in MC subjects: significant caveolar EC activity (long arrows).